Variability ~~of~~ in the properties of the distribution of the relative humidity with respect to ice: Implications for contrail formation

Sidiki Sanogo[1], Olivier Boucher[1], Nicolas Bellouin[1,2], Audran Borella[1], Kevin Wolf[1], and Susanne Rohs[3]

[1]Institut Pierre–Simon Laplace, Sorbonne Université / CNRS, Paris, France
[2]Department of Meteorology, University of Reading, Reading, United Kingdom
[3]Forschungszentrum Jülich GmbH, Institute of Energy and Climate Research 8 – Troposphere, Jülich, Germany

Correspondence: Sidiki Sanogo (sidiki.sanogo@ipsl.fr) and Olivier Boucher (olivier.boucher@ipsl.fr)

Abstract.

Relative humidity with respect to ice (RHi) is a key variable in the formation of cirrus clouds and contrails. We document its probability density function (PDF) using long-term Measurement of ~~Ozone~~ OZone and water vapour on ~~Airbus aircraft~~ AIrbus airCraft In-service programme (MOZAIC) and the In-service Aircraft for a Global Observing System (IAGOS) observations over the period 1995-2022 in the upper troposphere (UT) and lower stratosphere (LS) between 325 hPa and 175 hPa. The characteristics of the RHi PDF differ in the UT and in LS of the high-latitudes (HL) and mid-latitudes (ML) regions of the Northern Hemisphere. In the LS, ~~the probability (P) of observing a certain RHi~~ this PDF decreases exponentially with increasing RHi. ~~The rate of this decrease in P with increasing RHi is greater in supersaturated than in subsaturated conditions.~~ In the UT, ~~P~~ it first increases exponentially ~~under~~ in subsaturated conditions then decreases exponentially in supersaturated conditions. Because of these different behaviours, the PDF for the combined UT and LS is bimodal. In contrast to the HL and the ML regions, ~~P~~ the RHi PDF in the tropical troposphere decreases exponentially with increasing RHi. The different forms of PDF, in the tropics and in the higher latitude regions~~(ML and HL)~~, lead to a global PDF of RHi in subsaturated tropospheric conditions that is almost uniform. ~~This PDF shows a weak mode in the vicinity of 100 %, which can be associated essentially with the presence of cirrus clouds. These different characteristics of the RHi PDF exhibit some differences depending on the pressure level.~~ These findings invite caution when using MOZAIC and IAGOS measurements to calibrate large-scale simulations of RHi. The variability of RHi properties associated with that of ~~the temperature~~ temperature also has implications for the formation of contrails. We examined the impact of switching ~~from the current fuel of aircraft, kerosene ,~~ fuel (from kerosene to bio-ethanol ~~, or to~~ or liquid-hydrogen) on the frequency of ~~contrails~~ contrail formation using the Schmidt-Appleman criterion. We show that bio-ethanol and ~~more so hydrogen~~ to a larger extent liquid-hydrogen would produce more contrails. The impact of a potential change from kerosene to ~~one of these two~~ these alternative fuels decreases with ~~the decreasing pressure level~~ decreasing pressure but increases when moving from the high-latitudes of the Northern Hemisphere to the tropics. ~~We recommend that the comparison between models and observations be performed regionally and for the UT and LS separately.~~ Finally, we emphasize that investigations ~~on~~ of the impact on ~~the contrail occurrence~~ contrail occurrence frequency of switching from fossil kerosene to more sustainable fuels must be carried out in various ~~climatic~~ meteorological conditions.

1 Introduction

Water vapour ~~is a trace gas~~ in the Earth's atmosphere ~~(Meerkötter and Vázquez-Navarro, 2012) but~~ is responsible for two-thirds of the natural greenhouse effect ~~(Gierens et al., 2012). It is also responsible for one-sixth of the energy transport from~~ (Peixoto and Oort, 1992). It plays an important role in the transport of energy from the Earth's surface into the atmosphere via evapotranspiration of water at the ground and condensation and freezing in the atmosphere (Gierens et al., 2012). A ~~variable used~~ convenient variable to analyze the condensation and freezing processes at play in ~~in situ~~ in-situ cirrus clouds and contrails formation is the Relative Humidity with respect to ice (RHi). ~~Cases~~ Situations where RHi is 100 % are ~~labelled~~ said to be "saturated with respect to ice". ~~In~~ It is common for water vapour to be ice supersaturated (RHi $>$ 100 %) in the upper troposphere (UT) and lower stratosphere (LS)~~region (UTLS) and also sometimes near the surface in Antaretica , RHi can be ice supersaturated (RHi $>$ 100 %)~~ , but also in the lower troposphere in Antarctica (Gierens et al., 1999; Gierens and Brinkop, 2012; Genthon et al., 2017; Petzold et al., 2020).

Ice supersaturation occurrence is a prerequisite for the formation of ~~in situ~~ in-situ natural cirrus and ~~contrail-cirrus (Schumann, 1996; Hey . In situ~~ persistent contrails (Schumann, 1996; Heymsfield et al., 2017). In-situ cirrus clouds may form in the UT and in the LS via homogeneous nucleation at temperature colder than –38 °C and ~~ice supersaturations~~ RHi above 140 % ~~are then necessary (Kanji et al., 2017; Heymsfield et al., 2017)~~is then necessary (Heymsfield et al., 2017; Kanji et al., 2017). Cirrus clouds may also form via heterogeneous freezing at temperatures lower than 0 °C with ~~ice supersaturation~~ RHi above 100 % in the presence of ice nucleating particles ~~(Kanji et al., 2017; Heymsfield et al., 2017)~~(Heymsfield et al., 2017; Kanji et al., 2017). The formation ~~mechanisms of contrails are~~ mechanism of contrails is quite different to those of natural cirrus. ~~They~~ Contrails are linked to the atmospheric conditions that influence the complex processes occurring in the wake of aircraft ~~(Schumann, 1996; Kärcher, 2018)~~ (Schumann, 1996; Kärcher, 2018). Schmidt (1941) and Appleman (1953) provided a simple thermodynamic criterion, known as the Schmidt–Appleman criterion (SAc), which ~~bypasses~~ approximates the complex dynamical processes and ~~only based~~ is based only on ambient temperature and relative humidity. It has been amended by Schumann (1996), taking into account fuel combustion properties and the aircraft engine propulsion efficiency (see ~~Sect.~~ Section 2.4 for a refresher on the criterion).

~~Contrail-cirrus~~ Contrails can evolve into ice clouds, known as contrail-cirrus (Kärcher, 2018). Like natural cirrus, contrail-cirrus have a radiative forcing that is of relevance ~~for~~ to the Earth's climate ~~(Kärcher, 2018; Schumann et al., 2021; Lee et al., 2021)~~ (Kärcher, 2018; Lee et al., 2021; Schumann et al., 2021). They interact with both solar and terrestrial radiation and the net effect is a warming of the ~~troposphere~~ climate system (Lee et al., 2021). However, there is a large spread in the net radiative forcing for individual ~~contrail cirrus~~ contrail-cirrus and the average magnitude of this effect is still uncertain. For instance, for the year 2018, the Effective Radiative Forcing (ERF) of contrail-cirrus in high-humidity regions was estimated to be 57.4 mW m^{-2} with a 5-95 % likelihood range of 17 to 98 mW m^{-2} (Lee et al., 2021). This non-CO_2 forcing of aviation ~~is~~ might be stronger than that from CO_2 (34.3 mW m^{-2} ~~)~~with a 5-95 % likelihood range of 31 to 38 mW m^{-2}) (Lee et al., 2021). Overall, the uncertainty associated with the ERF of contrails and contrail-cirrus represents a significant part of the uncertainty associated with the total ERF of aviation on the Earth's climate (Lee et al., 2021). ~~Natural cirrus clouds play an important role in~~ A further uncertainty regarding the climate impact of contrail-cirrus relates to their efficacy in warming the Earth's ~~radiative~~

budget (Fusina et al., 2007; Boucher et al., 2013)surface. Some studies (e.g., Ponater et al., 2021; Bickel, 2023) suggest that their efficacity might be lower than 1, meaning that contrail radiative forcing may be less efficient at causing surface temperature change than CO_2 radiative forcing.

Accurate representation of the Ice SuperSaturation Regions (ISSR) in numerical weather prediction models is important to improve the prediction of contrail-prone conditionspersistent contrails, which is important for mitigation strategies aiming to reduce the climate impact of the aviation sector through contrail avoidance (Sperber and Gierens, 2023). This first requires a good characterization of the spatial and temporal distribution of RHi. For this purpose, the characterization of ISSR (corresponding to the upper tail of the RHi distribution) has been carried out in some past studies (e.g., Petzold et al., 2020; Gierens et al., 1999). ISSR distributions have past studies (e.g., Gierens et al., 1999; Petzold et al., 2020). The frequency of occurrence of ISSR has been shown to depend on the location and season. In terms of spatial variability, the highest frequency is observed in deep convection regions of in the tropics above 200 hPa (Spichtinger et al., 2003b; Lamquin et al., 2012; Spichtinger et al., 2003a) (Spichtinger et al., 2003a, b; Lamquin et al., 2012). ISSR are more frequent at 400-300300-200 hPa and 300-200400-300 hPa in the mid and high-latitude regions, respectively (Lamquin et al., 2012). In terms of seasonality, their the highest frequency of occurrence in the Nortern Hemisphere mid-latitude regions is observed in winter, followed by spring, while they are less frequent in summer and autumn (Petzold et al., 2020; Spichtinger et al., 2003b; Lamquin et al., 2012; Wolf et al., 2023) (Petzold et al., 2020; Wolf et al., 2023). On a global scale, the seasonality of ISSR frequency shows spatial disparities depending on pressure level (see Fig. 10 in Lamquin et al. (2012)). It should be noted that the magnitude of the ISSR frequency depend of occurrence depends on the observational products being considered (e.g., airborne or spaceborne observations) due to differences in observation methods and their horizontal and vertical resolutions. Analysis using the European research programme MOZAIC showed that, on average in the troposphere an aircraft above 300 hPa has a 20-30 % and 35-40 % probability of encountering an ISSR in summer and in winter respectively, when flying over North America, the North Atlantic and Europe (Petzold et al., 2020). So, the average spatial distribution of ISSR is fairly well documented in the literature. However, the occurrence of contrails depend also also depends on the ambient temperature, the fuel combustion properties and the engine propulsion efficiency (Schumann, 1996).

The Probability Density Function (PDF) of RHi has also been analysed in several studies (e.g., Diao et al., 2014; Lamquin et al., 2012; Sm (e.g., Lamquin et al., 2012; Diao et al., 2014; Smit et al., 2014; Petzold et al., 2020) based on in situ measurements. They all found a bimodal PDF with a first mode between 0 and 10 % and a second mode between 95 and 112 %. However, there is still a gap in our knowledge on of the properties of the tropospheric and stratospheric PDFs of RHi. Gierens et al. (1999) showed that the large scale PDF of RHi in the UT and LS are different at 250 and 200 hPa. The PDF of RHi in the LS follows an exponential decay in both ice supersaturation and subsaturationboth below and above saturation, and therefore does not show any break in slope in the vicinity of 100 %, unlike in the UT. A local scale study of Spichtinger et al. (2003a)over Lindenberg (Germany) reported that like in the UT, contradicting findings of Spichtinger et al. (2003a), indicate that the RHi PDF in the LS exhibits a break in slope in the vicinity of 100 % . It should also be noted that the over the location of Lindenberg (Germany) using radiosonde observations. The question of how these properties vary between the tropics and the mid and high-latitudes regions, and also with pressurelevel, has so far not been fully answered.

The In this context, the objectives of this study are twofold: 1) to document the properties of the PDF of RHi in the UT and in the LS, in both clear and cloudy conditions as a function of the latitude and pressure, 2) to document using the Schmidt-Appleman criterion the occurrence frequency of the frequency of occurrence of conditions favorable to the formation of non-persistent and persistent contrails and the impact of a fuel change on these frequencies using the Schmidt-Appleman criterion.

This article is structured as follows. Section 2 details the dataset used in the present study and describes our methodology. Section 3 documents the properties of the PDF of RHi and the occurrence frequency of frequency of occurrence of the conditions favorable to contrail formation. Finally, Section 4 summarizes our main findings.

2 Data and methods

2.1 Dataset from IAGOS and MOZAIC passenger aircraft

We analyzed RHi from airborne measurements spanning for the period 1995 to 2022. Measurements of ambient temperature (T) and pressure (p), relative humidy humidity with respect to liquid water (RHl), ozone volume mixing ratio (m_{0_3}), and ice crystal number concentration (N_i) are also analysed either to understand the properties of the PDF of RHi or to document the frequency of the conditions favorable to the formation of contrails. They are all obtained from the Measurement of Ozone OZone and water vapour on Airbus aircraft AIrbus airCraft In-service (MOZAIC) programme (Marenco et al., 1998) over the period 1995-2014 and from the In-service Aircraft for a Global Observing System (IAGOS) programme (Petzold et al., 2015) over the period 2011-2022. Data for N_i are available only from a subset of the IAGOS flights. The MOZAIC and IAGOS data are measured with a temporal sampling of 4 seconds. In this study, for each flight we used the latest version (amongst versions file version 3.1.1 to 3.1.4) data available at the time of our study.

Figure 1 shows the spatio-temporal distribution of RHi measurements in the Upper Troposphere - Lower Stratosphere (UTLS) defined here as the pressure layer between 325 hPa and 175 hPadefined here as the UTLS region. The best sampled areas are in the Mid-Latitudes (ML) of the northern Northern Hemisphere. They are the Eastern United States of America (40°N – 60°N, 120°W – 65°W, USA hereafter), Europe (40°N – 60°N, 5°W – 30°E, EU hereafter) and especially the North Atlantic corridor (40°N – 60°N, 65°W – 5°W, NA thereafter). The sampling Sampling over Russia, Asia, the High-Latitudes (HL) of the northern Northern Hemisphere and in the tropics is less dense. Our study is focused on the HL, ML, and the tropics. The areas area of the ML spanning from USA to EU is analysed more in in a longitude range from the USA to Europe is analysed in more detail. The geographical coordinates of the different study areas are provided in Table 1. For documenting the PDF of RHi, we considered data above 325 hPa then split by splitting the UTLS into three layers 325-275 hPa, 275-225 hPa and 225-175 hPa using a resolution of 50 hPa. Most measurements are performed in the 275-225 hPa and 225-175 hPa layers (Fig. 2). Those performed in 325-275 hPa are less prominent numerous (Fig. 2) but they represent 186812, 4963539, 2980377 measurements in the HL, the ML, and in the tropics, respectively.

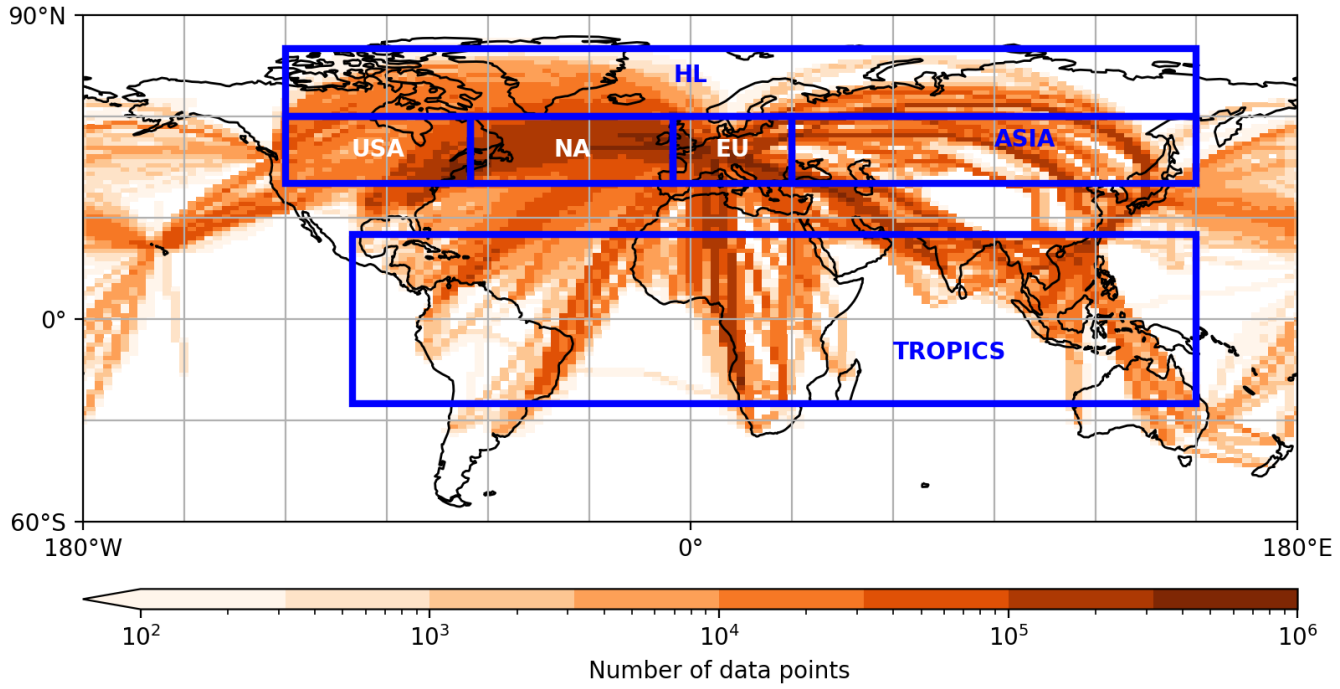

Figure 1. Global coverage of RHi observations by MOZAIC and IAGOS aircraft over the 1995-2022 period, between 325 ~~hPa~~ and 175 hPa shown as the total number of measurements per 2.5° × 2.5° gridbox (log scale). The areas delimited by blue boxes represent the study ~~zones~~areas. Their coordinates are provided in ~~the~~ Table 1.

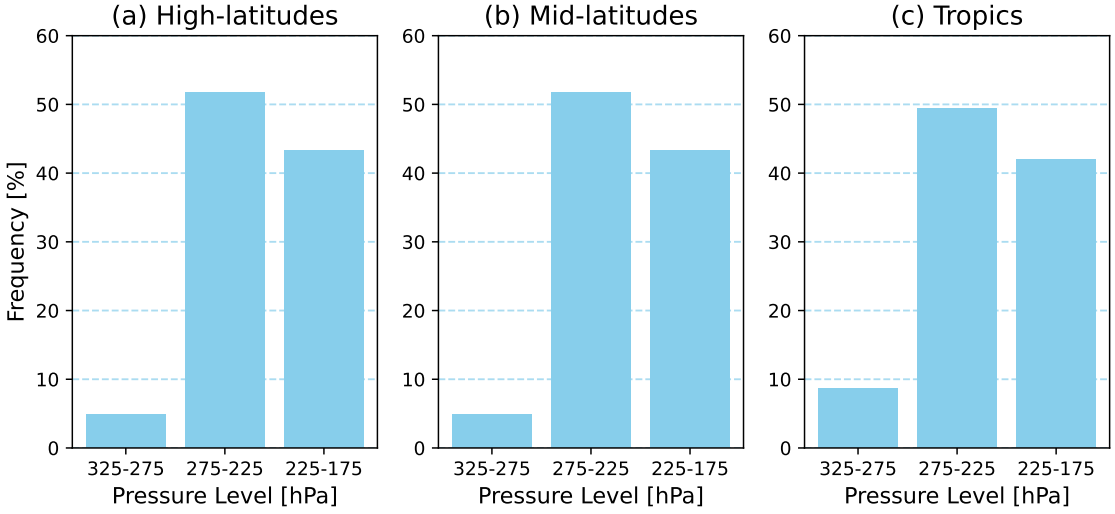

Figure 2. ~~Frequency~~ Relative frequency of RHi measurements per ~~range of~~ pressure ~~level~~ layer in ~~the~~ a) the high-latitudes, b) the mid-latitudes of the Northern Hemisphere and c) ~~in~~ the tropics over the period 1995-2022.

Table 1. Names of study areas and their geographical coordinates.

~~Names~~ Study areas	Latitude and longitude ranges
High-Latitudes (HL)	60°N – 80°N, 120°W – 150°E
Mid-Latitudes (ML)	40°N – 60°N, 120°W – 150°E
~~Eastern~~ United States of America (USA)	40°N – 60°N, 105°W – 65°W
North Atlantic (NA)	40°N – 60°N, 65°W – 5°W
Europe (EU)	40°N – 60°N, 5°W – 30°E
Tropics	25°S – 25°N, 100°W – 150°E

2.2 Data selection

MOZAIC and IAGOS data are assigned different quality levels, ranging from "good" to "not validated". In this study, only "good" measurements of RHi, RHl, T, p, m_{0_3}, and N_i are considered. ~~A~~ It should be noted that, between the years 2011 and 2017, there was a grounding problem with the IAGOS data acquisition system~~affected RHi between 2011 and 2017. During~~ . For this period, ~~RHi values are selected~~ the quality flag of RHi is not well derived but it is known to be similar to that of RHl. We therefore selected RHi values using the RHl quality flag ~~. We followed~~ for this particular period. We follow Gierens et al. (1999) by separating UT ~~air mass measurements~~ and LS air mass measurements on the ~~based~~ basis of their m_{0_3}. The mean value of the ozone mixing ratio m_{0_3} at the thermal tropopause being 130 ppb with a standard deviation of 92 ppb (Duhnke et al., 1998), we consider that measurements are from a UT air mass if $m_{0_3} < 130$ ppb and ~~a~~ an LS air mass otherwise. This approach is used for a ~~fairly comparaison~~ comparison of our results to those of Gierens et al. (1999). ~~It is worth noting that a~~ A sensitivity analysis using the threshold of 2 potential vorticity ~~unit data of~~ units as simulated by the fifth generation of the European Centre for Medium-Range Weather Forecasts atmospheric reanalysis (ERA5) to discriminate tropospheric and stratospheric measurements showed consistent results with the m_{0_3} based approach (not shown).

2.3 Differentiation of clear sky and cloudy conditions

The N_i variable is used to differentiate ~~data~~ observations measured in cirrus clouds from those in clear sky conditions. Different thresholds are used in the literature. For instance, Beswick et al. (2015) and Lloyd et al. (2020) used a threshold of 0.05 particles cm^{-3} while Petzold et al. (2017) used a lower threshold of 0.015 particles cm^{-3}. Here we used an even smaller threshold of 0.001 particles cm^{-3}, i.e, we considered ~~as in cloud measurements those with~~ cloud measurements to have $N_i \geq 0.001$ particles cm^{-3}. We used this threshold to be more restrictive ~~on~~ in the discrimination of the clear conditions for the investigations of the origin of the wet mode in the PDF of RHi. We then ~~used the~~ perform a sensitivity test with thresholds of 0.015 particles cm^{-3} and 0.05 particles cm^{-3} ~~for sensitivity test since a~~ since the threshold of 0.001 cm^{-3} is associated with detection uncertainties that can exceed 50 % ~~is associated with the threshold of 0.001 cm^{-3}~~ (Petzold et al., 2017). To exclude potential measurements in the presence of supercooled liquid water, as in Petzold et al. (2017), we considered only N_i data for which the temperature is colder than –40 °C, which corresponds to the threshold for the ~~spontaneous~~ homogeneous freezing of water

droplets (Petzold et al., 2017). ~~Due to~~ Because of low sampling of the HL by IAGOS aircraft equipped with N_i measurement sensors, the analysis involving screening clear and cloudy conditions is restricted only to the ML and to the tropics.

2.4 Contrail detection: Schmidt-Appleman criterion

The combustion of kerosene (or alternative fuels) releases hot and humid air behind the aircraft, which is progressively diluted in the cold and dry ambient atmosphere. This mixture follows a line in a $p - T$ diagram (Schumann, 1996). ~~If RHi of the mixture is subsaturated, while T is colder than a critical ambient temperature~~ In this framework, non-persistent contrails form at ambient temperature below a critical value T_{crit} and RHl ~~is higer than a critical value~~ larger than RHl_{crit} ~~, the non-persistent contrails form~~ (Schumann, 1996). Contrails are persistent if RHi is ~~ice supersaturated~~ above 100% (See Fig. 3 in Schumann, 1996). We used this criterion known as SAc to document the frequency of non-persistent and persistent contrails formation as a function of the pressure ~~level~~ for the following fuels: kerosene, bio-ethanol (ethanol, hereafter) and liquid-hydrogen (hydrogen, hereafter).

The approximation of T_{crit} frequently used in the literature (e.g., Rap et al., 2010) is given by the following equation:

$$T_{crit} = 226.69 + 9.43 \cdot \ln(G - 0.053) + 0.7272 \cdot \ln^2(G - 0.053) \quad (1)$$

where G (in $\text{Pa}\,\text{K}^{-1}$) is the slope of the mixture line in the $p - T$ diagram and is defined as follows:

$$G = \frac{EI_{H_2O} \cdot c_p \cdot p}{\epsilon \cdot Q(1 - \eta)} \quad (2)$$

G combines the atmospheric properties (the ambient pressure (in Pa) of the flight altitude, the isobaric heat capacity of air c_p = 1004 $\text{J}\,\text{kg}^{-1}\,\text{K}^{-1}$, and the ratio of the molecular masses of water vapour and dry air $\epsilon \approx 0.622$), the fuel properties (the specific combustion heat of the fuel Q (in $\text{J}\,\text{kg}^{-1}$) and the emission index of water vapour for the fuels EI_{H_2O} (in $\text{kg}\,\text{kg}^{-1}$)) and the aircraft engine propulsion efficiency of the aircraft η. In this study, we consider η = 0.3 which corresponds to a typical present-day fleet value (Schumann, 1996, 2012).

The values of Q and EI_{H_2O} for the different fuels are listed in Schumann (1996) and in Wolf et al. (2023).

The ~~RHl_{crit} threshold~~ RHl_{crit} threshold for an ambient temperature T is determined by:

$$RHl_{crit} = \frac{G \cdot (T - T_{crit}) + e_{sat}^{liq}(T_{crit})}{e_{sat}^{liq}(T)} \quad (3)$$

where e_{sat}^{liq} is the saturation water vapour pressure. For more details, the reader should refers for example to Schumann (1996) and Rap et al. (2010).

3 Results

3.1 Number of ice crystals in cirrus clouds

~~Values of RHi~~ Situations that are ice supersaturated and subsaturated are observed in both clear and cloudy conditions (Kahn et al., 2009; Krämer et al., 2009, 2016; Petzold et al., 2017). Therefore, for a better characterization of the PDF of RHi, we first document how clear and cloudy conditions are sampled in IAGOS measurements. For this purpose, we used three different detection thresholds (0.001, 0.015, 0.05 particles cm^{-3}) for characterizing clouds, based on their ice crystal number concentration N_i (see ~~Sect.~~Section 2.3). We found, consistently with Petzold et al. (2017), that IAGOS aircraft encounter cirrus clouds with larger N_i in the tropics than in the ML (Fig. 3). ~~63-56 % and 47-30 % of the observed~~ Considering only non-zero N_i ~~in cirrus clouds are respectively greater than~~ values, the percentages of datapoints above the thresholds of 0.015 (0.05) particles cm^{-3} are 63 (47) % and 56 (40) % for the 275-225 and ~~0.05 particles cm^{-3}, in the pressure range 275-175 hPa~~ 225-175 hPa layers, respectively in the tropics (Fig. 3). In the ML, the ~~percentage of $N_i \geq$ 0.015 particles cm^{-3} and $N_i \geq$ 0.05 particles cm^{-3} in 325-275 hPa and in 275-225 hPa~~ percentages are 58 ~~% and~~ (38) % for the 325-275 hPa layer, 40 ~~%, respectively~~ (20) % for the 275-225 hPa layer (Fig. 3). The highest fraction of $N_i < 0.015$ cm^{-3} in ML is observed at the altitudes of 225-175 hPa~~. It represents~~ , with a value of 72 % ~~of the observed N_i~~ (Fig. 3). The higher N_i in cirrus clouds in the tropics compared to the ML between 275-175 hPa is consistent with the findings of studies using synergetic lidar-radar satellite data (e.g., Sourdeval et al., 2018) and can be explained by the fact that, in the tropical region, strong updrafts in convective regions ~~producing high ice supersaturation~~ produce ice supersaturation and cause high nucleation rates that lead to high number concentrations of ice crystals (Krämer et al., 2016).

Table 2. Number of ~~total measurements~~ datapoints (~~collocated~~ with ~~measurements of~~ ambient temperature lower than –40 °C) including a measurement of the ice crystals number concentration (N_i) and ~~the~~ percentage of ~~total measurements,~~ datapoints for which $N_i \geq$ 0.001 ~~particles cm^{-3}~~, ~~$N_i \geq$~~ 0.015 ~~particles cm^{-3} and $N_i \geq$~~, 0.05 particles cm^{-3} in the mid-latitudes (ML) of the Northern Hemisphere and in the tropics over the period 2011-2022.

Regions	Mid-latitudes			Tropics	
Pressure ranges (hPa)	325-275	275-225	225-175	275-225	225-175
Total number of ~~measurements~~ datapoints with T < –40 °C	155620	2905616	4402016	1539032	4502899
Fraction of ~~measurements~~ datapoints ($N_i \geq$ 0.001 particles cm^{-3})	6.0 %	3.7 %	1.8 %	4.4 %	8.2 %
Fraction of ~~measurements~~ datapoints ($N_i \geq$ 0.015 particles cm^{-3})	3.5 %	1.4 %	0.5 %	2.7 %	4.6 %
Fraction of ~~measurements~~ datapoints ($N_i \geq$ 0.05 particles cm^{-3})	2.0 %	0.7 %	0.2 %	2.0 %	3.3 %

3.2 How ~~long~~ often do IAGOS aircraft fly in cirrus clouds?

The fractions of aicraft flying time in cirrus clouds are presented in Table 2. They are computed for each pressure ~~range~~ layer as the number of measurements of N_i collocated with measurements of temperature lower than –40 °C that are at least equal to the cirrus detection threshold divided by the total number of measurements. These fractions can also be interpreted as cirrus occurrence frequencies as seen by IAGOS.

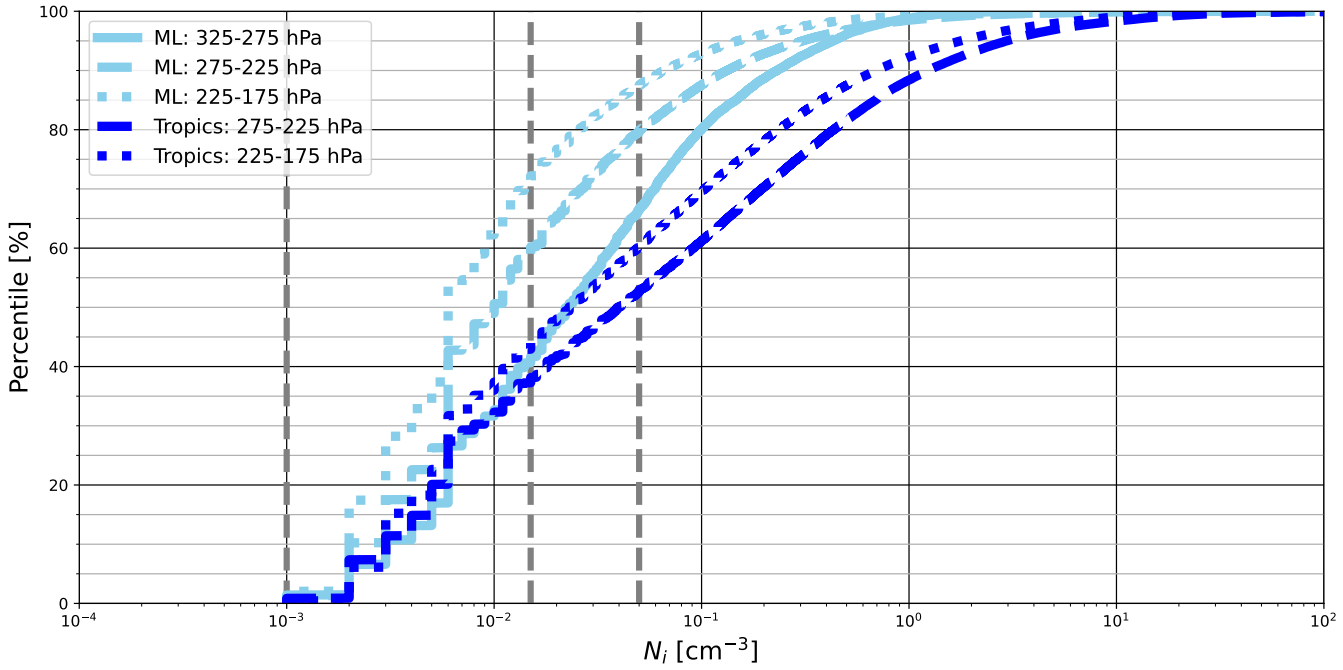

Figure 3. ~~Ice~~ Cumulative PDF of the ice crystal ~~number concentrations~~ in the mid-latitudes (ML) of the Northern Hemisphere and in the tropics over the period 2011-2022 for different pressure layers. The vertical dashed gray lines correspond to the concentration thresholds of 0.001~~cm^{-3}~~, 0.015 ~~cm^{-3}~~ and 0.05 cm^{-3} (see Text).

~~In 275-225 hPa and 225-175 hPa pressure ranges, the~~ The occurrence frequency of cirrus clouds decreases in the ML with ~~pressure level~~ decreasing pressure (when going from 275-225 to 225-175 hPa) while it increases in the tropics. Using 0.001 particles cm^{-3} as a threshold, we determined fractions of 4.4% and 8.2% in the tropics and 3.7 % to 1.8 % in the ML (Table 2). On average, the total occurrence frequency of cirrus is highest in the tropics (Table 2). This is consistent with the findings of Petzold et al. (2017) who showed that IAGOS data capture the global pattern of cirrus clouds. When the detection threshold is increased to 0.015 particles cm^{-3} and 0.05 particles cm^{-3}, ~~the cirrus clouds~~ cirrus cloud occurrence frequency decreases, in particular in the 225-175 hPa layer (Table 2), but remains ~~relevant~~large. This suggests that the properties of RHi PDF from MOZAIC and IAGOS ~~data are~~ measurements correspond to a combination of clear-sky and cloudy-sky conditions.

3.3 Characteristics of the RHi probability density function

3.3.1 Upper troposphere

Gierens et al. (1999) showed that over larger spatial ~~and longer timescales~~scales and longer time scales, the distributions of ~~subsaturated and supersaturated RHi~~ RHi smaller and larger than 100 % in the UT follow a uniform law and an exponential law, respectively. RHi is however modulated in space and time by ~~absolute~~ fluctuations in specific humidity and temperature

fluctuations (Diao et al., 2014). Consequently, statistical distribution of RHi will be its statistical distribution is subject to spatial variability. This is illustrated in Fig. 4 that shows the PDF of RHi in the ML, the HL and in the tropics, for the pressure ranges 325-275, 275-225 and 225-175 hPa pressure layers. In the ML, the characteristics of the RHi PDF depend on the pressure level. It is unimodal in 325-275 hPa with a mode at 108 % (Fig. 4d) while it is bimodal in the 275-225 and 225-175 hPa layers. The two modes in 275-225 hPa are centered at 5 % and 108 % (Fig. 4e) while those in 225-175 hPa are located at 8 % and 100 % (Fig. 4f). The existence or the magnitude of the dry mode in the 275-225 and 225-175 hPa layers in the ML is not certain. It may correspond to LS measurements, erroneously attributed to the UT because of uncertainties in the method for discriminating UT and LS measurements of RHi. We therefore focused the following analysis on the RHi values greater than 25 %. It should be noted that the The presence of a wet mode is was reported in the early study of Spichtinger et al. (2003a) based on radiosoundings over Lindenberg (Germany). In agreement with Reutter et al. (2020) who analyzed RHi in the North Atlantic, the mean and the standard deviation of RHi distributions in the UT vary little with the pressure level in the ML (Table 3). However, their variations are substantial in the tropical and HL regions (Table 3).

An important point, common to these UT RHi PDF distributions and consistently with Gierens et al. (1999), is that the probability (P) of observing a certain PDF decreases exponentially with increasing RHi beyond a supersaturated value S (here, $S \in [100\ \%, 110\ \%]$)decreases exponentially with increasing RHi. For a quantitative intercomparison of the part of the RHi PDF corresponding to RHi $\geq S$, we take $S = 100\ \%$, and as Gierens et al. (1999), we fit each PDF using the following straight line:

$$\ln P(RHiPDF) \approx a + b \cdot \text{RHi} \tag{4}$$

in which a is the intercept and b is the slope. For the three different pressure intervalslayers, b (multiplied by 100 for easier readinglegibility) is close to -4 and a is between 2 and 3 in the ML (Table 4). The PDF of subsaturated values of RHi have different characteristics . The probability P of observing has different characteristics in the range of RHi that correspond to subsaturation. The PDF of RHi $\in [25\ \%, 100\ \%[$ increases ($b \geq 0$), instead of decreasing exponentially with increasing RHi in the 275-225 and 225-175 hPa layers (Table 4). In the 325-275 hPa layer, the PDF is nearly uniform ($b \approx 0$) for RHi $\in [25\ \%, 100\ \%[$ (Table 4). Comparing The comparison of USA, North Atlantic, and Europe revealed that, at reveals that, in the first order, the distribution distributions of RHi over the three regions are consistent with each other for in the 275-225 and 225-175 hPa layers (Fig. 5). However, substantial differences appear for in the 325-275 hPa layer. The magnitude of the dry mode at these pressure levels is higher in the USA compared to the other two areas (Fig. 5), for all seasons (see Fig. S1 in the Supplementary Material). In addition, the probability of observing PDF of RHi between 25 % and 100 % is almost uniform over Europe, while it increases and decreases exponentially over the Nord North Atlantic and USA, respectively (Fig. 5). This implies differences between the three sub-regions in the mechanisms that modulate RHi variability in the pressure range 325-275 hPa. Weak Insufficient sampling may also be a contributing factor, since fewer measurements were made at these pressure levels (Fig. 2).

The UT RHi ~~PDF~~ PDFs in the HL exhibit similar features to those in the ML (Fig. 4a-c). ~~For~~ However, for RHi between 25 % and 100 %, the exponential ~~increasing rate~~ rate of increase b is slightly higher for the HL than for the ML (Fig. 4a-f, Table 4).

In the tropical region, the evolution of the ~~PDF of the RHi with pressure level~~ RHi PDF with pressure is different (Fig. 4g-i). The PDFs are bimodal and in contrast to the ML and the HL, the magnitude of the dry mode decreases with ~~pressure level~~ increasing pressure (i.e going down in the atmosphere) while that of the wet mode increases. This is due to the warm tropical temperatures, which ~~favours low RHi values~~ favour low RHi for 325-275 hPa despite the higher availability of water vapour compared to the other two pressure ~~ranges~~ layers considered here. Unlike the ML and the HL, the existence of a mode between 0 ~~%~~ and 25 % is ~~probably real~~ more certain in the tropics since the measurements analyzed are less affected by stratospheric measurements. For RHi $\geq$ 25 %, the PDF is characterised by an exponential decay on both sides of the mode at 100 %. ~~It should however be noted that the~~ The characteristics of the PDF ~~beyond~~ above 100 % are similar to those of the RHi PDF in the ML and HL. The important difference is that the absolute value of the rate parameter b decreases with decreasing pressure in the tropics, whereas it increases in ML and HL (Table 4). It is worth noting that the global PDF ~~of RHi includes these~~ (PDF combining RHi measurements in HL, ML and tropics) includes opposing tendencies in the ~~probability of occurrence of RHi values~~ PDF of RHi lower than 100 % between the tropics and the Northern Hemisphere~~into~~, resulting in an almost uniform PDF ($b \approx 0$, Fig. 4j-l). These results are consistent with the findings of Gierens et al. (1999).

Table 3. Long-term (1995-2022) mean and standard deviation of the ~~tropospheric and stratospheric~~ RHI values in the UT (and in ~~brackets~~the LS) in the High and Mid-Latitudes of the North Hemisphere ~~(denoted ML and HL respectively)~~ and in the tropics.

RHi PDF parameters	Mean (%)			Standard deviation (%)		
Regions	High-Latitudes	Mid-Latitudes	Tropics	High-Latitudes	Mid-Latitudes	Tropics
325 - 275 hPa	88.9 (33.0)	71.5 (31.3)	27.0	38.6 (23.9)	33.7 (23.1)	35.2
275 - 225 hPa	48.6 (24.4)	78.4 (28.4)	34.2	48.6 (23.7)	32.2 (25.4)	18.8
225 - 175 hPa	56.9 (30.7)	69.8 (24.5)	38.8	56.9 (22.5)	36.4 (24.7)	33.8

3.3.2 Lower stratosphere

In this section, we document the RHi PDF in the LS. This analysis is carried out only in the ML and the HL ~~since~~ because in MOZAIC and IAGOS stratospheric measurements are very few in the 325-175 hPa layer in the tropics. ~~Mean RHi decrease~~ The mean RHi decreases with decreasing pressure ~~level~~ in the ML and HL while ~~the~~ its standard deviation varies very little (Table 3). Reutter et al. (2020) found similar results over the North Atlantic Ocean.

~~Since the~~ The observed temperature in the UT and the LS are relatively close, ~~while little water vapour crosses the tropopause (Reutter et al., 2020; Petzold et al., 2020),~~ but water vapour transport into the LS through the tropopause is low (Petzold et al., 2020; Reutte . This makes the mean value of RHi lower in the LS ~~is lower~~ than in the UT. Another important difference ~~with the troposphere~~between the LS and the UT, common to the ~~two regions~~ ML and the HL and to the three pressure ~~ranges~~ layers considered here, is that

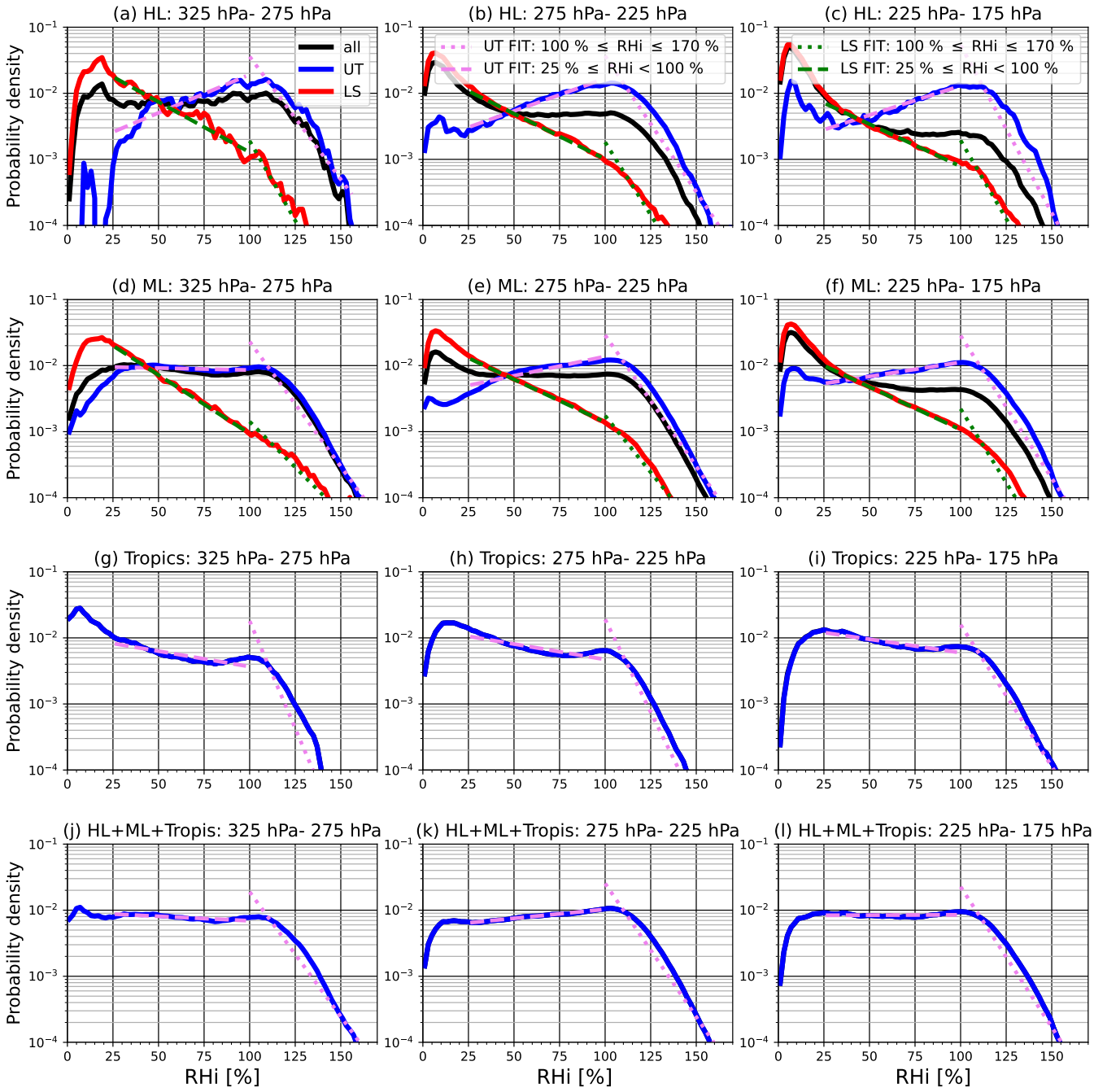

Figure 4. Probability density function of the relative humidity with respect to ice (in %) computed over the period 1995-2022 for the pressure ~~ranges~~ layers 325-275 ~~hPa~~, 275-225 ~~hPa,~~ and 225-175 ~~h~~Pa, a-c) in the High-Latitudes (HL) of the Northern Hemisphere, d-f) in the Mid-Latitudes (ML) of the Northern Hemisphere~~(ML)~~, g-i) for the tropical region, j-l) the PDF of the three domains combined. For each pressure ~~range~~layer, the tropospheric RHi PDF (blue), the stratospheric RHi PDF (red) and their combined PDF (black) are shown. The green dashed and dotted lines correspond to the fit for RHi $\in$ [25 %, 100 %[and for RHi $\in$ [100 %, 170 %[, respectively, in the stratosphere. The ~~violet~~ pink dashed and dotted lines are those for the troposphere.

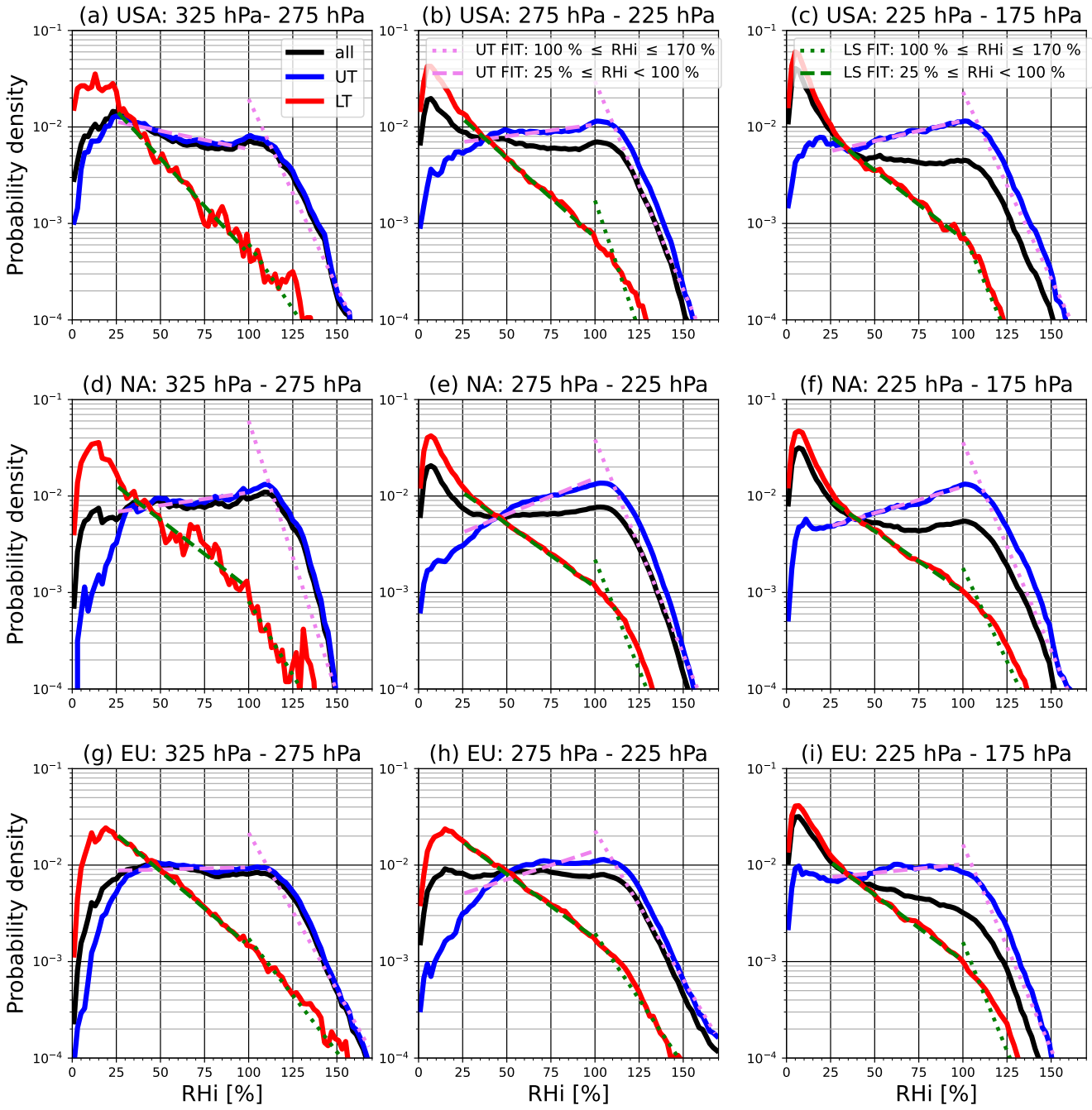

Figure 5. Same as Fig. 4 but for the ~~Eastern~~ North America (USA), the North Atlantic (NA), and ~~Western~~ Europe (EU).

Table 4. Values (with uncertainty range of ± 1 standard deviation) of the parameters a and b of the fit ~~line~~ lines (see Eq. 4) ~~of~~ in the ~~RHi supersatured values~~ supersaturated (top) and ~~the~~ subsaturated ~~values~~ (bottom) part of the RHi distribution in the UT, computed over the period 1995-2022. The values of b are multiplied by 100 for the sake of legibility.

Fit parameters	a			$100 \cdot b$		
Regions	High-Latitudes	Mid-Latitudes	Tropics	High-Latitudes	Mid-Latitudes	Tropics
325 - 275 hPa	2.3 ± 0.24 -2.9 ± 0.04	2.1 ± 0.12 -2.0 ± 0.01	4.3 ± 0.48 -1.9 ± 0.02	-3.7 ± 0.18 1.21 ± 0.07	-3.7 ± 0.09 0.00 ± 0.01	-6.1 ± 0.04 -0.45 ± 0.00
275 - 225 hPa	2.7 ± 0.16 -2.7 ± 0.01	2.3 ± 0.10 -2.4 ± 0.01	3.7 ± 0.18 -1.8 ± 0.02	-4.1 ± 0.011 0.09 ± 0.01	-3.8 ± 0.07 0.06 ± 0.02	-5.4 ± 0.04 -0.48 ± 0.00
225 - 175 hPa	3.8 ± 0.29 -2.7 ± 0.02	2.7 ± 0.13 -2.4 ± 0.00	2.0 ± 0.09 -1.8 ± 0.01	-5.1 ± 0.21 0.08 ± 0.03	-4.3 ± 0.01 0.04 ± 0.00	-3.9 ± 0.04 -0.41 ± 0.00

~~the probability of observing a specific~~ in the LS, the PDF of RHi greater than 25 % decreases exponentially with increasing RHi (Fig. 4a-f, Table 5). This exponentially decaying PDF of RHi in the LS, with a break in the slope around 100 %, is a feature reported by Spichtinger et al. (2003a) over Lindenberg (Germany). Our results show that this property is common to the RHi PDF in the ML and the HL of the Northern Hemisphere ~~.~~ in the 275-225 and 225-175 hPa layers (Fig. 4b,c,e,f). For these pressure layers, Gierens et al. (1999) did not find the break in slope around 100 % in the MOZAIC data for the period 1995-1997. This might be due to an undersampling of the LS properties of RHi PDF over ~~this period~~ the period they considered. It is ~~the case here for the stratospheric PDF of RHi~~ worth noting that in the 325-275~~hPa layer ($b \approx 0$,~~ hPa layer, the break in slope around 100 % in the RHi PDF in the LS is marked only in the HL (Fig. 4a~~,c,~~). In the ML, the break in slope seems to be undersampled in the USA in the MOZAIC and IAGOS data (Fig. 5a~~,d,g). It is important to note that, similarly to the UT, the probability of observing a supersaturated RHi increases with decreasing pressure. It should also be noted that~~). In the LS, unlike the UT, the dry mode between 0 % and 25 % ~~in the LS~~ is expected due to ~~its~~ the low water vapour content (see Petzold et al. (2020)).

3.3.3 Lower stratosphere and upper troposphere

As shown above, there are differences between the shapes of RHi PDF in the UT and in LS in the HL and in the ML. In this section, we analyzed the properties that emerge when UT and LS are ~~not separated~~considered together. Such an approach is used in several studies (e.g., Lamquin et al., 2012; Smit et al., 2014; Diao et al., 2014; Petzold et al., 2020). We found, in agreement with these studies that the RHi PDF in the UTLS is bimodal (Fig. 4a-f). The ~~dry~~ mode of the ~~PDF of RHi~~ RHi PDF between 0 % and ∼50 % (depending on pressure ~~range~~ layer and region) is essentially a characteristic of the LS while that for RHi greater than ∼50 % is dominated by the features of the RHi PDF in the UT (Fig. 4a-f). The magnitude of the dry mode varies with the pressure level. It increases when going up from 325 to 175 hPa in the LS (Fig. 4a-f) since at these pressure levels in the LS, water vapour ~~content decreases whereas~~ decreases while the temperature increases (Reutter et al.,

Table 5. Same as Table 4 but for the ~~lower stratosphere~~LS.

Fit parameters	a		$100 \cdot b$	
Regions	High-Latitudes	Mid–Latitudes	High-Latitudes	Mid-Latitudes
325 - 275 hPa	1.2 ± 0.34 -1.3 ± 0.03	-0.2 ± 0.09 -1.2 ± 0.01	-4.0 ± 0.29 -1.5 ± 0.05	-2.6 ± 0.06 -1.8 ± 0.01
275 - 225 hPa	1.4 ± 0.16 -1.6 ± 0.00	0.8 ± 0.04 -1.5 ± 0.04	-4.1 ± 0.12 -1.3 ± 0.01	-3.6 ± 0.04 -1.3 ± 0.00
225 - 175 hPa	1.7 ± 0.18 -1.8 ± 0.01	1.8 ± 0.13 -1.8 ± 0.01	-4.4 ± 0.14 -1.2 ± 0.02	$-4.4 \pm$ ~~009~~ 0.09 $-1.2 \pm$ 0.01

2020; Petzold et al., 2020). ~~It should be noted that the~~ The RHi PDF of the ML includes more UT measurements than the RHi PDF of the HL since the pressure level of the tropopause increases (~~the~~ i.e. its altitude decreases) with latitude. Consquently, the shape of the upper tail of the RHi PDF is more dominated by the tropospheric PDF in the ML than in the HL (Fig. 5). In the ML, some differences can be noted at the sub-regional scale on the shape of the RHi PDF. The exact ranges of the lower/upper tail of the PDF of RHi dominated by the LS/UT features ~~RHi~~ depend on the location (Fig. ~~5~~4).

3.3.4 Clear vs cloudy conditions

To further document the RHi PDF, we compared its properties in clear and cirrus cloud conditions between 325-175 hPa in the ML and in the tropics using the sub-sample of data measured onboard aircraft equipped with ice crystal number concentration measuring sensor. In these two regions, the ~~aformentioned~~ aforementioned wet mode, in the vicinity of 100 % in the RHi PDF that combines clear and cloudy conditions ~~comes~~ appears to come essentially from cirrus clouds (Fig. 6). Conditions with $N_i < 0.001$ particles cm^{-3} associated with the slow and complex processes of cirrus clouds formation and dissipation may also contribute. Consequently, this mode ~~is not completly inexistent~~ also partly appears in clear sky conditions depending on the region. In the subsample of the IAGOS data analysed here, it is more prominent in the tropics than in the ML (Fig. 6a-c). Petzold et al. (2017) conducted similar analyses in different regions including, areas in the tropics and ML regions using IAGOS data of the period from July 2014 to October ~~2015 and found that~~ 2015. They found that the RHi wet mode in the tropical Atlantic is more prominent (see their Fig. 8b). This characteristic seems to be smoothed out in satellite and radar-lidar synergistic data, since Kahn et al. (2009) and Lamquin et al. (2012) reported no ~~peaks~~ mode in the vicinity of 100% under clear conditions.

In addition to the mode around 100 %, the PDF of in-cloud RHi also shows a dry mode between 0 and 50 % (Fig. 6a,c) which could correspond to a measurement artifact. The positions of the ~~in-cloud RHi mode in~~ mode around 100 % are different between the ML and ~~in the tropics are different~~ the tropics (Fig. 6a-c). It is subsaturated in the tropics while it is supersaturated in the ML (Fig. 6a-b). Cirrus clouds ~~exhibit ice-subsaturated~~ can exhibit ice subsaturated and ice supersaturated

conditions depending on ~~their state of life~~ the stage of their life cycle (Petzold et al., 2020; Li et al., 2023). Some studies ~~(e.g., Petzold et al., 2017; Krämer et al., 2009) have then~~ (e.g., Krämer et al., 2009; Petzold et al., 2017) have found that the mode of the PDF of RHi in cirrus clouds is ice supersaturated while others ~~(e.g., Li et al., 2023; Ovarlez et al., 2002; Kahn et al., 2009)~~ (e.g., Kahn et al., 2009; Ovarlez et al., 2002; Li et al., 2023) found an ice ~~sub-saturated mode. Figure 6c shows that the subsample of IAGOS flight data analyzed here sampled tropical cirrus clouds, characterized by essentially by undersaturated RHi. These cases may correspond to cirrus clouds in the dissipation phase. However, since the level of supersaturation of this humid mode of RHi depends~~ subsaturated mode. Since the magnitude and position of this wet mode depend on the region as illustrated in this study and reported in the literature, further studies are needed to better characterize it and elucidate the mechanisms involved.

The PDF of in-cloud RHi decreases with RHi for subsaturated conditions but increases with RHi for supersaturated conditions when increasing the detection threshold (Fig. 6). This is consistent with the fact that, more generally, high concentrations of ice crystals are associated with high RHi (Petzold et al., 2017; Krämer et al., 2016). The lower tail of the PDF of RHi could include measurements in contrails or at the bottom of cirrus clouds where subsaturated conditions are observed more often (Dekoutsidis et al., 2023). They may also correspond to measurements carried out in diluted cirrus clouds or in the proximity of cirrus clouds where ice crystals may be mixed with clear air by turbulence. Erroneous measurements may also contribute since the uncertainties associated with these thresholds are large (more than 50 % for the threshold of 0.001 cm^{-3} particles, see Section 2.3).

3.4 Implications of RHi variability for contrail formation

3.4.1 Frequency of ice supersaturation regions

~~Subsequently~~In this section, we investigate the frequency of occurrence of ISSR, which are necessary for persistent contrail formation (Schmidt, 1941; Appleman, 1953). We computed this frequency as the ratio of aircraft flight time in ISSR to total flight time. The frequency of ISSR collocated with measurements of temperature lower than –38 °C (temperatures at which cirrus clouds may form by homogeneous nucleation, see Section 1) is presented in Fig. 7 while that with no restriction on the temperature is presented in Fig. 8. The difference between these two frequencies is low (less than 3 %) except for the 325-275 hPa layer in the tropics, where it is relatively high (6 %). In the HL and in the ML, ISSR frequency decreases with the pressure level (Fig. 8a-c). In the HL, for the 325-275, 275-225, 225-175 hPa layers, the occurrence frequencies of ISSR with no restriction on the temperature are respectively 19.2 %, 11.0 %, 5.5 %, while they are ~~20.8~~21 %, ~~17.6~~17.8 % and 9.0 % in the ML. In the tropics, ISSR occur more frequently (~~15.5~~15.6 % of the time) in the ~~pressure range of~~ 225-175 hPa layer. In the 325-275 and 275-225 hPa layers they occur ~~7.9~~8 % and 10.4 % of the time, respectively. It should be noted that, ~~whether in the tropics or in the mid or high-latitudes~~ for the three regions, the frequency of ISSR is characterized by regional and seasonal variability~~which is well documented in the literature (see Sect. 1).~~. In the tropics (for the 325-275, 275-225, 225-175 hPa layers) and in the ML (for the 325-275 hPa layer), MOZAIC and IAGOS aircraft flying time in the ISSR is highest in winter and lowest in summer (Fig. 7b-c). In the three pressure layers in the HL and for the 225-175 hPa layer in the ML, the frequency

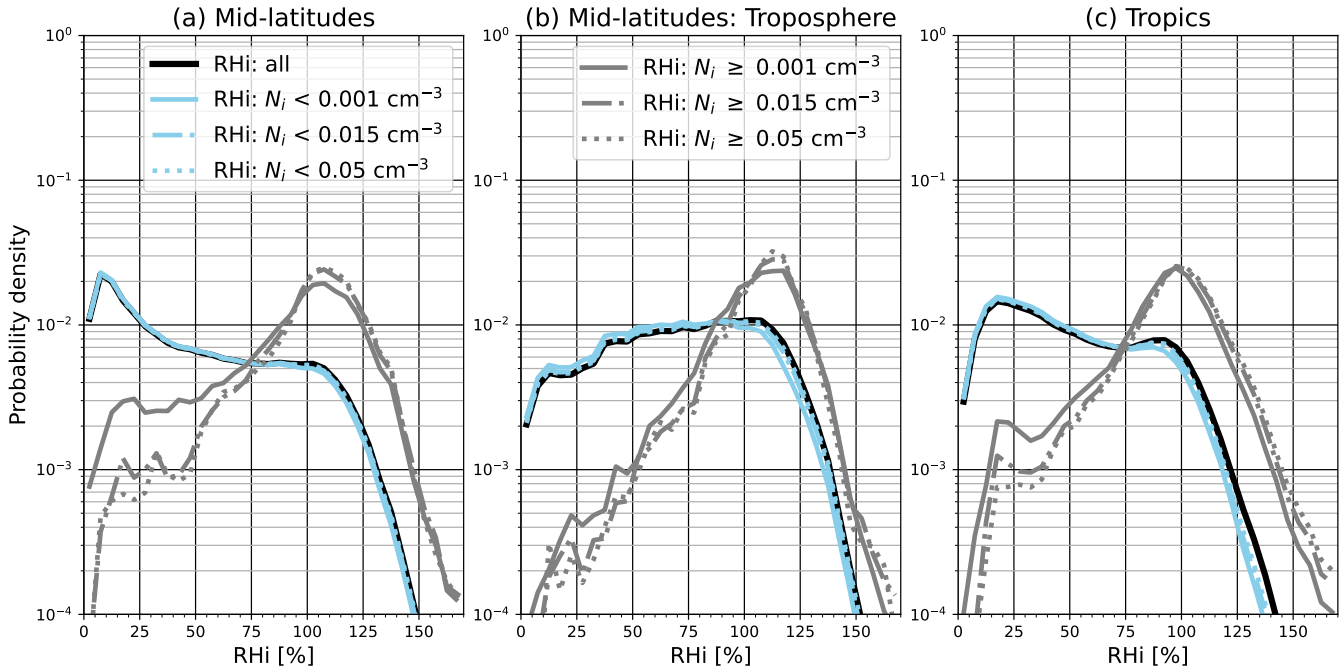

Figure 6. Probability density function of RHi in ~~the~~ clear ~~conditions~~ (sky blue) and cloudy ~~sky~~ (gray), and in ~~the total conditions~~ all-sky (black) conditions, a) in the upper troposphere and lower stratosphere in the mid-latitudes of the Northern Hemisphere, b) only in the upper troposphere in the mid-latitudes of the Northern Hemisphere and c) in the tropical upper troposphere and lower stratosphere, computed over the period 2011-2022. Only RHi measurements collocated with measurements of temperature lower than –40°C are ~~plotted~~used in the analysis.

of ISSR seems to be essentially driven by the seasonal evolution of LS conditions (Fig. 7a-b; see also Fig. S2), which are drier than UT conditions. In the Northern Hemisphere, the altitude of the tropopause is lower in winter and spring than in summer and autumn (Liu et al., 2014). As a result, LS air masses are sampled by MOZAIC and IAGOS aircraft more frequently in winter and spring than in summer and autumn (Fig. S2). In the 275-225 hPa layer in the ML, the seasonality of ISSR frequency is less marked (Fig. 7b). In the 325-275 hPa layer, ISSR seasonality seems to follow that of temperature (Fig. 7b). In line with Lamquin et al. (2012) findings, the seasonality of ISSR frequency combining tropospheric and stratospheric conditions varies as a function of latitude and pressure.

3.4.2 Frequency of contrail formation and fuel choice

Investigations are being carried out by the aviation industry ~~on~~ about the possibility of using bio-ethanol (ethanol, hereafter) and liquid-hydrogen (hydrogen, hereafter) as ~~an alternative fuel~~ alternative fuels to kerosene. Ethanol and hydrogen are two ~~of the so-called Sustainable Aviation Fuel (SAF). SAF~~ fuels that could qualify as sustainable aviation fuel, and whose use is expected to reduce aviation-induced CO_2 emissions if they are generated from carbon-neutral sources (Ng et al., 2021). They

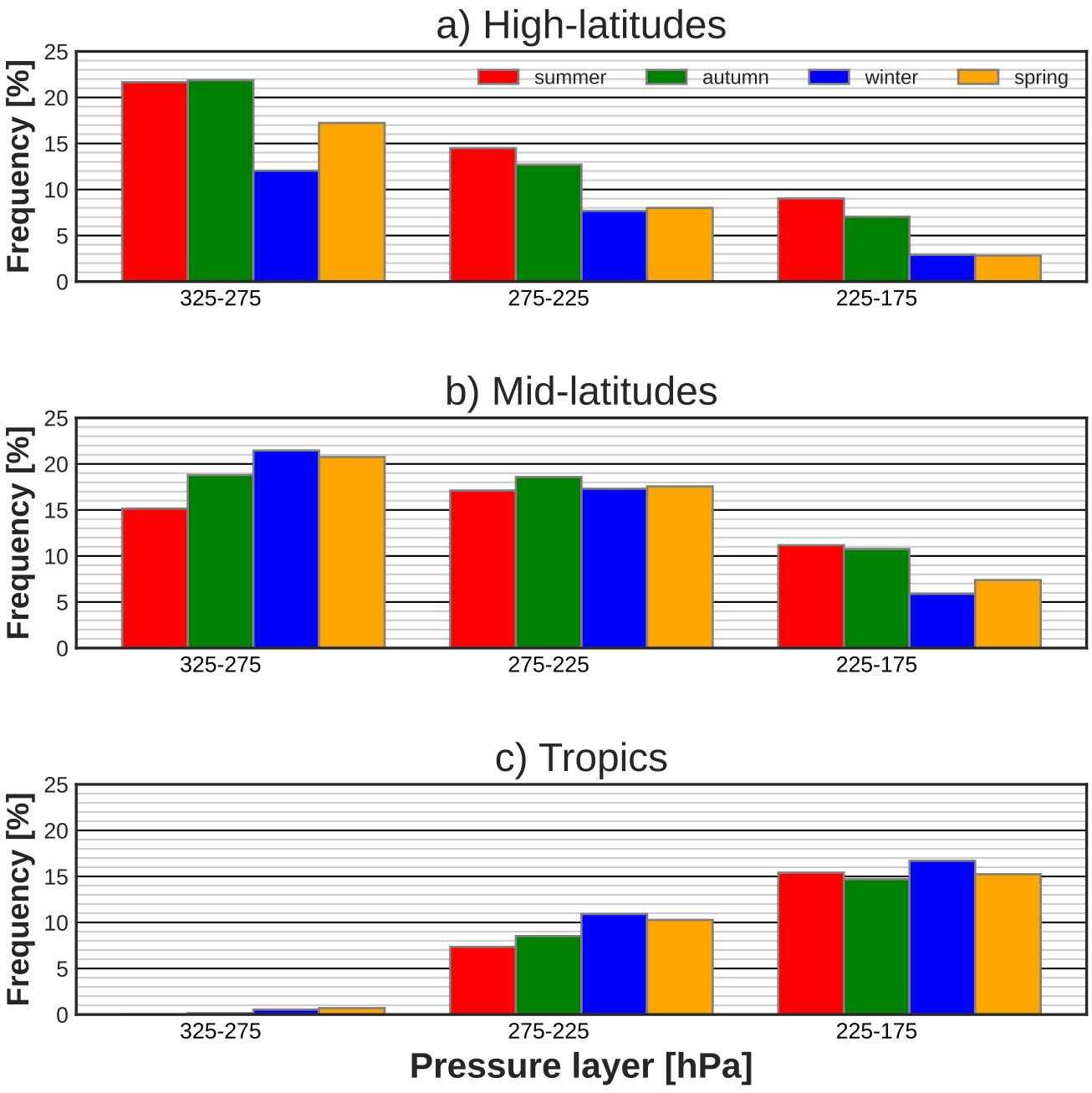

Figure 7. Frequency of ISSR (in %) for four seasons (color bars) and three pressure layers when considering only measurements with temperature lower than –38°C for a) the high and b) the mid-latitudes of the Northern Hemisphere c) and the tropics.

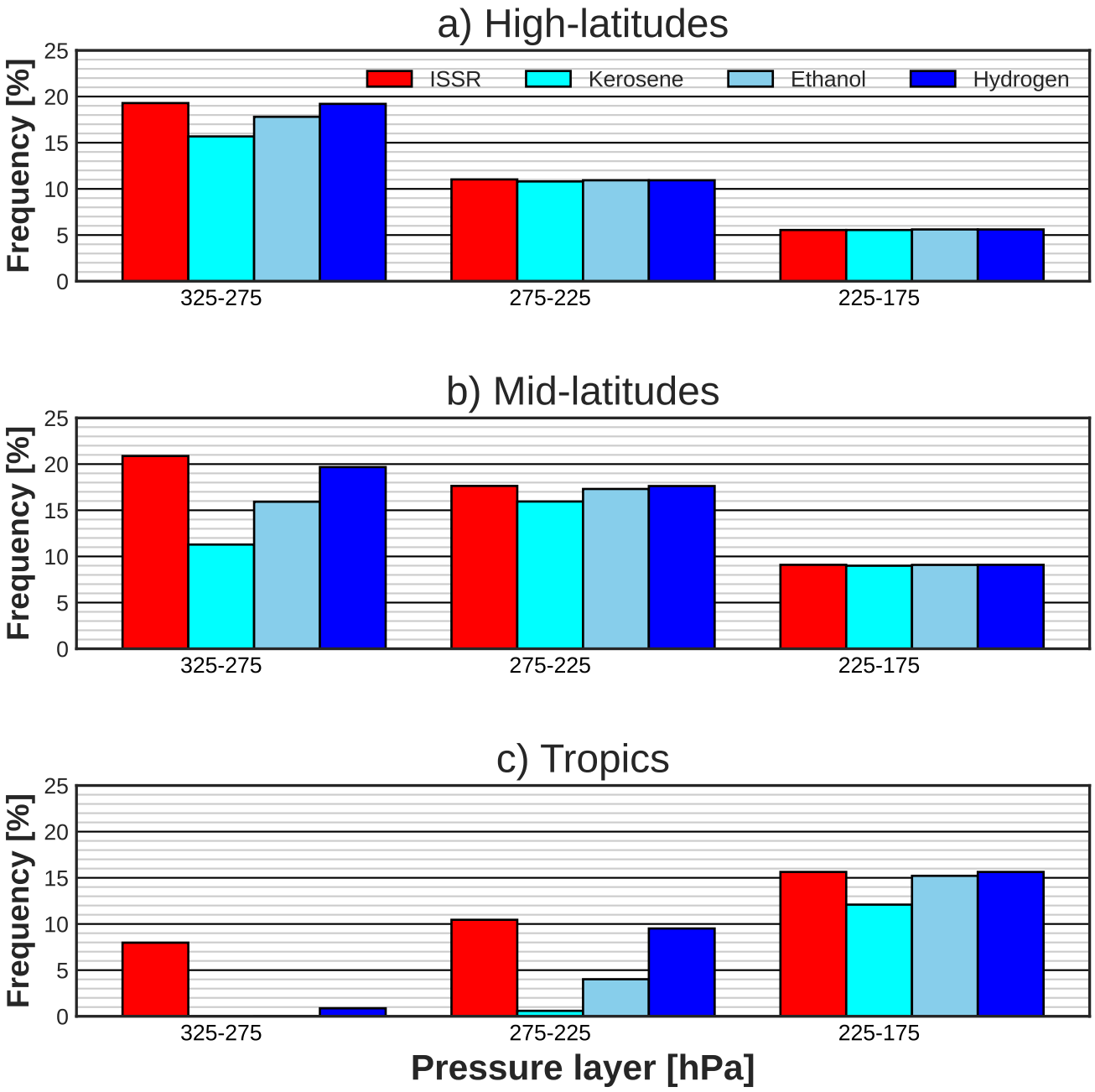

Figure 8. ~~Frequency~~ Annual average frequency (%) of ISSR (~~in cyan~~red) and of persistent contrail formation conditions for three pressure layers for kerosene (~~sky blye~~cyan), ~~liquid ethanol~~ bio-ethanol (~~red~~sky blue) and ~~hydrogen~~ liquid-hydrogen (blue) fuels over the a) high and b) mid-latitudes of the Northern Hemisphere and over c) the tropics.

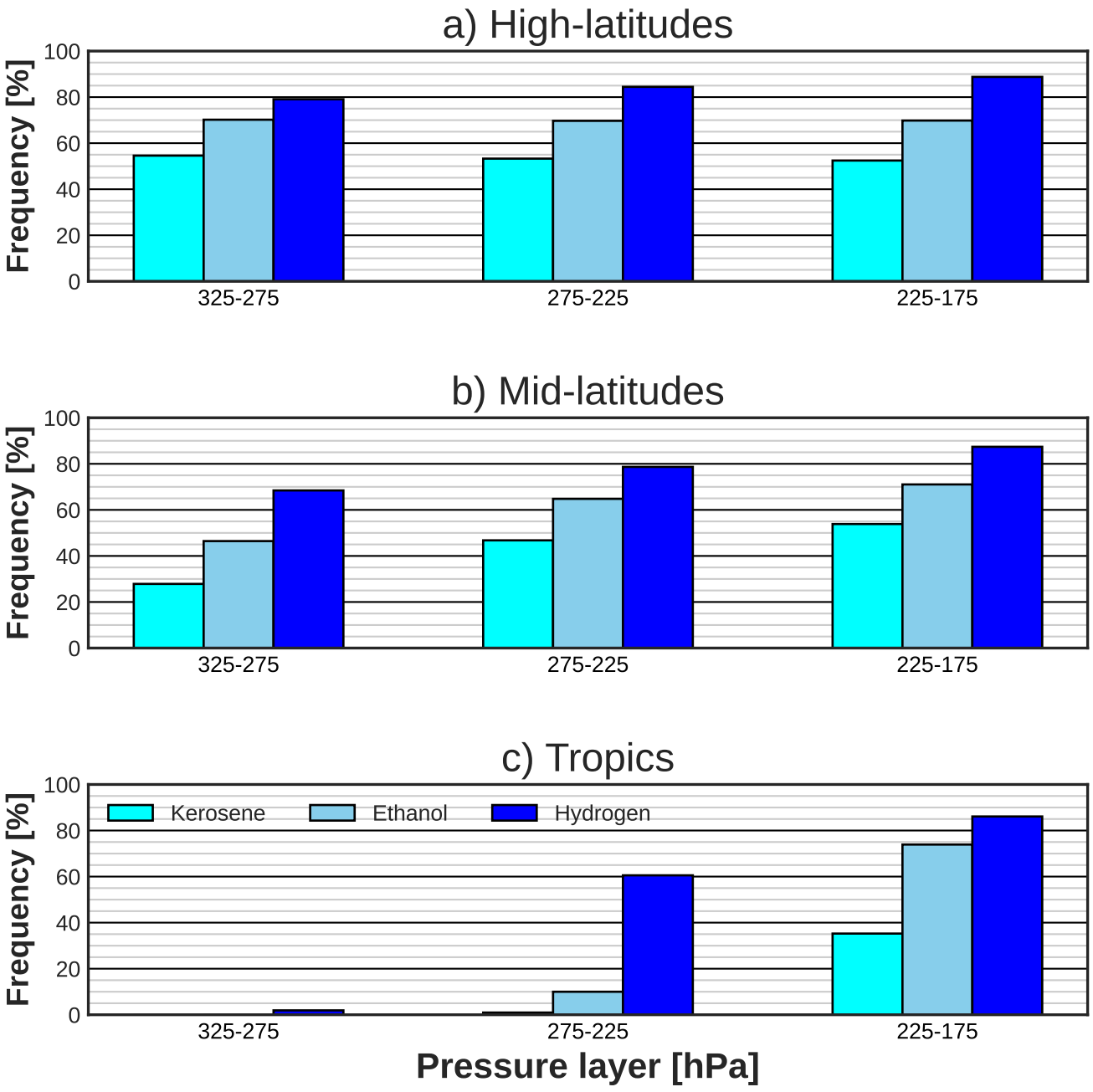

Figure 9. ~~Frequency~~ Annual average frequency (%) of non-persistent contrail formation conditions for ~~with~~ three pressure layers for kerosene (~~sky blue~~cyan), ~~liquid ethanol~~ bio-ethanol (~~red~~sky blue) and ~~hydrogen~~ liquid-hydrogen (blue) fuels over the a) high and b) ~~mid latitudes~~ mid-latitudes of the Northern Hemisphere and over c) the tropics.

could however produce contrails which have a net warming effect on the climate (see ~~Sect.~~Section 1). Here, we used the SAc to test the impact of using ethanol or hydrogen on the formation of contrails compared to kerosene. The SAc also accounts for the aircraft-engine propulsion efficiency η (see ~~Sec.~~Section 2.4) which is expected to continue to increase in the future (Sahoo et al., 2020). But, since our study is focused only on the impact of fuel choice, we used a typical present-day aircraft-engine propulsion efficiency of 0.3. The SAc is applied to MOZAIC and IAGOS measurements, varying the specific combustion heat of the fuel Q and the emission index of water vapour for the EI_{H_2O} of kerosene, ethanol, and hydrogen. The values of Q and EI_{H_2O} are set to 43.2~~J~~ MJ kg^{-1} and 1.25 $kg\,kg^{-1}$ for kerosene, to 27.2~~J~~ MJ kg^{-1} and 1.17 $kg\,kg^{-1}$ for ethanol, to 120~~J~~ MJ kg^{-1} and 8.94 $kg\,kg^{-1}$ for hydrogen (Schumann, 1996; Wolf et al., 2023).

The fraction of flying time during which aircraft can produce persistent contrails as a function of the fuel used is shown in the Fig. 8. These fractions or frequencies depend on the region and the altitude of the flight. For instance, MOZAIC and IAGOS aircraft using kerosene and flying in the HL ~~at the altitude, corresponding to the pressure range~~ in the 325-275 hPa ~~,~~ pressure layer are estimated to have produced persistent contrails during ~~15.6~~15.8 % of the flight time (Fig. 8a). This frequency decreases to ~~10.8~~11 % and to 5.5 % for the 275-225 and 225-175 hPa layers, respectively. For the 325-275 hPa layer, MOZAIC and IAGOS aircraft would have formed persistent contrails more often if they had used hydrogen or ethanol (19.2 % and ~~17.8~~18 %, respectively) instead of kerosene, while the fuel used has almost no effect for the 225-175 hPa layer (Fig. 8a). ~~The comparison with the frequency of ISSR showed that for~~ Comparing ISSR frequency shows that for the 325-275 hPa ~~, with the kerosene aircraft~~ layer, aircraft that use kerosene fly in ice supersaturated air masses for ~~3.6~~3.4 % of the time without producing persistent contrails~~(Table ??)~~. This frequency is equal to ~~1.4~~1.2 % for ethanol ~~(Table ??)~~ and 0 % for ~~hyrogen~~ hydrogen indicating that with hydrogen fuel, persistent contrails would form as soon as ~~the~~ air masses are ice supersaturated. ~~Similar conclusions are found for the 275-175 hPa layer (Table ??~~The impact of the fuel choice is much weaker for the 275-225 hPa and 225-175 hPa layers (Fig. 8a).

Like in the HL, the impact on the formation of persistent contrails of switching from kerosene to ethanol or to hydrogen decreases with decreasing pressure ~~level in~~ in the ML. In this region, with kerosene as fuel, aircraft produce persistent contrails more frequently (for ~~15.94~~16 % of the flight time) ~~between~~ in the 275-225 hPa layer (Fig. 8b) which correspond to the pressure ~~ranges where they~~ range where aircraft fly most (Fig. 2). This occurrence frequency is about 11.3 % ~~between~~ in the 325-275 hPa ~~and 8.9 % between~~ layer and 9 % in the 225-175 hPa ~~(Fig. 8b). The frequencies of persistent contrails induced by hydrogen closely follow the ISSR frequencies~~ layer (Fig. 8b). Overall, the ~~fuel switching impact~~ impact of switching fuel is highest for 325-275 hPa and lowest for 225-175 hPa (Fig. 8b). ~~It is only with hydrogen that persistent contrails form at almost all the pressure ranges considered here as soon as ISSR conditions occur (Table ??).~~

~~Difference between the frequency of persistent contrails associated with the kerosene, the bio-ethanol and the liquid-hydrogen and the frequency of ice supersaturation, in the High and Mid-latitudes of the North Hemisphere (denoted HL and ML respectively) and in the tropics, computed over the period 1995-2022. Regions Fuels Kerosene Ethanol Hydrogen Kerosene Ethanol Hydrogen Kerosene Ethanol Hydrogen 325 - 275 hPa 3.6% 1.4% 0.0% 9.5% 4.9% 1.2% 7.9% 7.9% 7.1% 275 - 225 hPa 0.2% 0.0% 0.0% 1.6% 0.3% 0.0% 9.8% 6.4% 0.9% 225 - 175 hPa 0.0% 0.0% 0.0% 0.0% 0.0% 0.0% 3.5% 0.4% 0.0%~~

Persistent contrail occurrence as a function of fuel in the tropics increases with decreasing pressure~~level~~. More importantly, the impact of switching from kerosene to ethanol or ~~to~~ hydrogen is most important at pressure where aircraft fly the most (275-225 hPa) (Fig. 8c ~~,~~ and Fig. 2c). At these altitudes, persistent contrails occur ~~0.5~~0.7 % of the time with kerosene but would occur 4.0 % and 9.5 % of the time, respectively, with ethanol and hydrogen (Fig. 8c). ~~This impact~~ The change is also important ~~between~~ in the 225-175 hPa layer (Fig. 8c).

~~The temperature in the UTLS is on average, colder in the HL and in the ML~~ Overall, the differences in the impact of switching from kerosene to ethanol or to hydrogen are driven by temperature variability. The differences are higher in warmer seasons than in the ~~tropics (Alder et al., 2011). The Clausius-Clapeyron relationship indicates that the saturation vapour pressure with respect to ice and~~ colder seasons (see Table S1 to S3 in the Supplementary Material). At low ambient temperature, the contrail plume exceeds water saturation more readily due to the curvature of the vapour pressure curve, regardless of the fuel being considered. The contrail plume may stay subsaturated with respect to liquid water ~~increases with the temperature. That partly explains the variability with pressure level and latitude~~ if the ratio of EI_{H_2O} to Q is low. In such conditions, persistent contrails are less frequent with kerosene than with hydrogen and ethanol. With the warming of the upper troposphere expected as a result of climate change (Kumar et al., 2022), the impact of switching from kerosene to ethanol or ~~hydrogen. Combustion releases hot and humid air behind the aicraft, which is progressively diluted to the cold and dry ambient atmosphere.Consequently, the fuel whose having the higher ratio EI_{H_2O} and Q (here hydrogen and ethanol), assuming that the other parameters of the combustion remain equal, tends to form more persistent contrails at the highest temperatures~~to hydrogen on contrail formation frequency could further increase in the future, potentially affecting pressure layers (e.g., 225-175 hPa in the high and mid-latitudes) and seasons (winter and spring in the high and mid-latitudes) where it is low under present conditions.

The frequency of ~~non persistent~~ non-persistent contrail formation increases with latitude and ~~the pressure level~~ with decreasing pressure between 325 and 175 hPa (Fig. 9). At these pressure layers, the impact of switching from kerosene to ethanol or ~~hydrogen and is prominent~~ to hydrogen is largest in the tropics (Fig. 9) and in summer, followed by autumn for the three regions (not shown). Our results ~~extend~~ confirm and generalize those of Wolf et al. (2023) ~~,~~ who showed that the impact of switching from kerosene to ethanol or to hydrogen will be greater on the occurrence of non-persistent contrails than on persistent contrails ~~,~~ using radiosoundings in the Paris region.

4 Summary and conclusions

In the present study, we documented the properties of ~~RHi~~ the atmospheric RHi PDF over the period 1995-2022 using the long-term MOZAIC and IAGOS observations made onboard passenger aircraft. The frequency of the contrail formation conditions is also analysed. The analyses are carried out over the ~~high-latitudes (HL) and mid-latitude (ML)~~ HL and ML regions of the Northern Hemisphere and in the tropics, in the ~~upper troposphere (UT) and lower stratosphere (LS), between 325 and 175 hPaseparated~~ UT and LS. The UT and LS pressure layer (325-175 hPa) is split into three pressure ~~ranges~~ layers with a resolution of 50 hPa. ~~RHi properties are also documented in clear sky and in cirrus cloud conditions.~~ Measurements with ozone volume mixing ratio below 130 ppb were flagged as ~~have been measured in~~ belonging to the UT, while those ~~corresponding to~~

with ozone volume mixing ratio above 130 ppb are flagged as LS measurements. ~~We used the thresholds~~ RHi PDF properties are also documented in clear sky and in cirrus cloud conditions. We used ice crystal number concentrations thresholds of 0.001, 0.015 and 0.05 particles cm^{-3} ~~of the ice crystal number concentration N_i for cloud~~ for clouds detection. The contrail formation conditions have been detected using the Schmidt-Appleman criterion considering an aircraft-engine propulsion efficiency of 0.3. The main results ~~are the following~~of our analysis are as follows:

1. The cirrus ~~cloud~~ clouds fraction sampled by IAGOS aircraft depends on the detection threshold and the location. ~~The highest cirrus cloud frequency is observed in the tropics. This frequency can be interpreted as the IAGOS aicraft flying time in cirrus clouds . With the detection threshold of 0.001 particles cm^{-3}, the frequencies are 4.4 % and 8.2 % at aircraft cruising altitude for the 275-225 and 225-175 hPa layers, respectively. In the ML, these respective frequencies are respectively 3.7 % and 1.8 %. They are of the order of 2.7 % and 4.6 %~~ Cirrus clouds are more frequent in the tropics ~~, 14 % and 0.5 %~~ than in the ML ~~for the cirrus having at least a concentration of ice crystals number of 0.015 particles cm^{-3}. These frequencies are slightly lower if the detection threshold of 0.05 particles cm^{-3} is used~~and their frequency decreases if a higher detection threshold is chosen. Cirrus clouds are characterized by higher amount of ice supersaturation than clear sky, which shifts the ~~upper tail of the~~ overall RHi PDF towards more ice supersaturation with a peak around 100 %.

2. We characterized the PDF of RHi in the UT. In the HL, the ML and the tropics,the ~~probability of observing a certain RHi decreases exponentially ,~~ PDF decreases exponentially with increasing RHi in ice supersaturation conditions. In ~~sub-saturated conditions, the probability of observing a certain RHi~~ subsaturated conditions, it increases exponentially with RHi in the HL and the ML regions while it decreases exponentially in the tropics. Combining these different shapes of subsaturated RHi PDF in the tropics and in mid and high latitudes (ML and HL) ~~lead~~ leads to a global tropospheric RHi PDF that follows ~~a~~ an almost uniform distribution.

3. The ~~LS RHi PDF~~ RHi PDF in the LS is different from that in the UT in the HL and ML. ~~The probability of observing a given RHi~~ It decreases exponentially with increasing RHi in both sub- and supersaturated regions. However, slope of the decrease of the ~~decrease slope of the distribution is higher under saturated~~ PDF is higher for supersaturated conditions than subsaturated conditions. The combination of these different shapes of subsaturated RHi PDF in the LS and in the UT leads ~~a total bimodal PDF of RHi~~ to a bimodal PDF in the ML and in ~~the~~ HL.

4. The probability of forming non-persistent and persistent contrails by aircraft using bio-ethanol and ~~liquid hydrogen~~ liquid-hydrogen instead of kerosene ~~are~~ was also analysed. Both are candidate fuels for reducing the climate impact of aviation. We found that these alternative fuels are more likely to produce contrails than kerosene. However, the magnitude of their impact on persistent contrail formation depends on pressure level and latitude. In the HL of the Northern Hemisphere, switching from kerosene to liquid-hydrogen or bio-ethanol ~~is more likely to have~~ has very little impact on the persistent contrails frequency for the 275-225 ~~hPa~~ and 225-175 hPa layers. ~~In this region, aircraft~~ The reason is that, in the HL of the Northern Hemisphere, aircraft running on kerosene already form persistent contrails nearly

every time they encounter air masses that are supersaturated with respect to ice at these altitudes. The same conclusions are found for 225-175 hPa in the ML. Overall, the impact of switching from kerosene to ~~hydrogen~~ liquid-hydrogen or bio-ethanol on persistent contrail occurrence decreases ~~with the pressure level~~ from tropics to high-latitude regions. It decreases with pressure between 325 and 175 hPa ~~, and from the tropicsto high-latitudes region~~except in the tropics. The impact of switching from kerosene to ~~hydrogen~~ liquid-hydrogen will be more important ~~in~~ for non-persistent contrails.

This study updates and completes some aspects of the studies of Gierens et al. (1999) and Spichtinger et al. (2003a) on the characteristics of the RHi PDF. ~~It emphasizes that observation and model comparisons~~ We draw several recommendations from our study. Comparisons between models and observations need to be performed for UT and LS separately, and preferentially over different regions and pressure levels, distinguishing cloud-free and cloudy conditions. Models that are calibrated to reproduce the global RHi PDF from MOZAIC and IAGOS data ~~risk doing~~ may do so for the wrong reasons. Similarly, it is important that observing systems designed to monitor UTLS humidity ~~will need to be able~~ have the capability to distinguish UT from LS. This may be a challenge for satellite-based systems, which may not have a sufficiently good vertical resolution. Finally, studies on the impact on the contrail occurrence of switching from fossil kerosene to more sustainable fuels must be conducted in various ~~climatic conditions.~~ meteorological conditions.

Data availability. IAGOS data are available from the IAGOS data portal (https://doi.org/10.25326/20). We use IAGOS data accessed on 3 november 2023.

Author contributions. SS, OB and NB designed the study. SS carried out the analysis and the preparation of the manuscript. OB and AB helped with the analysis. OB, AB, NB, KW contributed to the preparation of the manuscript. SR provided the MOZAIC and IAGOS data.

Competing interests. The authors declare that they have no conflict of interest.

Acknowledgements. S. Sanogo, O. Boucher, N. Bellouin, A. Borella and K. Wolf acknowledge support from the French Ministère de la Transition écologique (grant no. DGAC 382 N2021-39), with support from France's Plan National de Relance et de Resilience (PNRR) and the European Union's NextGenerationEU. We acknowledge the strong support of the European Commission, Airbus and the airlines (Deutsche Lufthansa, Air France, Austrian, Air Namibia, Cathay Pacific, Iberia, China Airlines, Hawaiian Airlines, Eurowings Discover, and Air Canada) that have carried the MOZAIC or IAGOS equipment and performed the maintenance since 1994. IAGOS has been funded by the European Union projects IAGOS–DS and IAGOS–ERI. Additionally, IAGOS has been funded by INSU-CNRS (France), Météo-France, Université Paul Sabatier (Toulouse, France) and Research Center Jülich (FZJ, Jülich, Germany). The IAGOS database is supported in France by AERIS (https://www.aeris-data.fr)

References

Alder, J., Hostetler, S. W., Pollard, D., and Schmittner, A.: Evaluation of a present-day climate simulation with a new coupled atmosphere-ocean model GENMOM, Geoscientific Model Development, 4, 69–83, https://doi.org/10.5194/gmd-4-69-2011, 2011.

Appleman, H.: The formation of exhaust condensation trails by jet aircraft, Bull. Am. Soc., 34, 14–20, https://doi.org/10.1175/1520-0477-34.1.14, 1953.

Beswick, K., Baumgardner, D., Gallagher, M., Raga, G. B., Minnis, P., Spangenberg, D. A., Volz-Thomas, A., Nedelec, P., and Wang, K.-Y.: Properties of small cirrus ice crystals from commercial aircraft measurements and implications for flight operations, Tellus B, 67, 27 876, https://doi.org/10.3402/tellusb.v67.27876, 2015.

Bickel, M.: Climate impact of contrail cirrus, Ph.D. thesis, DLR-Forschungsbericht. DLR-FB-2023-14. Dissertation. Ludwig-Maximilians-Universität München. 133 S., https://doi.org/10.57676/mzmg-r403, 2023.

Boucher, O., Randall, D., Artaxo, P., Bretherton, C., Feingold, G., Forster, P., Kerminen, V.-M., Kondo, Y., Liao, H., Lohmann, U., et al.: Clouds and Aerosols, in: Climate change 2013: the physical science basis. Contribution of Working Group I to the Fifth Assessment Report of the Intergovernmental Panel on Climate Change, pp. 571–657, Cambridge University Press, Cambridge, UK, https://doi.org/10.1017/CBO9781107415324.016, 2013.

Dekoutsidis, G., Groß, S., Wirth, M., Krämer, M., and Rolf, C.: Characteristics of supersaturation in midlatitude cirrus clouds and their adjacent cloud-free air, Atmos. Chem. Phys., 23, 3103–3117, https://doi.org/10.5194/acp-23-3103-2023, 2023.

Diao, M., Zondlo, M. A., Heymsfield, A. J., Avallone, L., Paige, M., Beaton, S., Campos, T., and Rogers, D.: Cloud-scale ice-supersaturated regions spatially correlate with high water vapor heterogeneities, Atmos. Chem. Phys., 14, 2639–2656, https://doi.org/10.5194/acp-14-2639-2014, 2014.

Duhnke, K., Wefers, J., Speth, P., Kley, D., Marenco, A., and Smit, H. G.: Untersuchung der in MOZAIC gemessenen Ozon-und Wasserdampfverteilung im polaren Strahlstrom über dem Nordatlantik, Tech. rep., Forschungszentrum Jülich, https://juser.fz-juelich.de/record/864943, 1998.

Fusina, F., Spichtinger, P., and Lohmann, U.: Impact of ice supersaturated regions and thin cirrus on radiation in the midlatitudes, J. Geophys. Res., 112, https://doi.org/10.1029/2007JD008449, 2007.

Genthon, C., Piard, L., Vignon, E., Madeleine, J.-B., Casado, M., and Gallée, H.: Atmospheric moisture supersaturation in the near-surface atmosphere at Dome C, Antarctic Plateau, Atmos. Chem. Phys., 17, 691–704, https://doi.org/10.5194/acp-17-691-2017, 2017.

Gierens, K. and Brinkop, S.: Dynamical characteristics of ice supersaturated regions, Atmos. Chem. Phys., 12, 11 933–11 942, https://doi.org/10.5194/acp-12-11933-2012, 2012.

Gierens, K., Schumann, U., Helten, M., Smit, H., and Marenco, A.: A distribution law for relative humidity in the upper troposphere and lower stratosphere derived from three years of MOZAIC measurements, Annales Geophysicae, 17, 1218–1226, https://doi.org/10.1007/s00585-999-1218-7, 1999.

Gierens, K., Spichtinger, P., and Schumann, U.: Ice supersaturation, in: Atmospheric Physics: Background–Methods–Trends, pp. 135–150, Springer, 2012.

Heymsfield, A., Krämer, M., Luebke, A., Brown, P., Cziczo, D., Franklin, C., Lawson, P., Lohmann, U., McFarquhar, G., Ulanowski, Z., and Van Tricht, K.: Cirrus clouds, Meteor. Monogr., 58, 2.1–62.26, https://doi.org/10.1175/AMSMONOGRAPHS-D-16-0010.1, 2017.

Kahn, B. H., Gettelman, A., Fetzer, E. J., Eldering, A., and Liang, C. K.: Cloudy and clear-sky relative humidity in the upper troposphere observed by the A-train, J. Geophys. Res., 114, https://doi.org/10.1029/2009JD011738, 2009.

Kanji, Z. A., Ladino, L. A., Wex, H., Boose, Y., Burkert-Kohn, M., Cziczo, D. J., and Krämer, M.: Overview of ice nucleating particles, Meteor. Monogr., 58, 1.1–1.33, https://doi.org/10.1175/AMSMONOGRAPHS-D-16-0006.1, 2017.

Kärcher, B.: Formation and radiative forcing of contrail cirrus, Nat. Commun., 9, 1824, https://doi.org/10.1038/s41467-018-04068-0, 2018.

Krämer, M., Schiller, C., Afchine, A., Bauer, R., Gensch, I., Mangold, A., Schlicht, S., Spelten, N., Sitnikov, N., Borrmann, S., et al.: Ice supersaturations and cirrus cloud crystal numbers, Atmos. Chem. Phys, 9, 3505–3522, https://doi.org/10.5194/acp-9-3505-2009, 2009.

Krämer, M., Rolf, C., Luebke, A., Afchine, A., Spelten, N., Costa, A., Meyer, J., Zoeger, M., Smith, J., Herman, R. L., et al.: A microphysics guide to cirrus clouds–Part 1: Cirrus types, Atmos. Chem. Phys., 16, 3463–3483, https://doi.org/10.5194/acp-16-3463-2016, 2016.

Kumar, T. L., Durga, G. P., Aravindhavel, A., Barbosa, H., and Rao, D. N.: Analysis of tropospheric warming and stratospheric cooling in the present and future climate from the suite of CMIP6 models, Theor Appl Climatol, 149, 1717–1726, https://doi.org/10.1007/s00704-022-04136-y, 2022.

Lamquin, N., Stubenrauch, C., Gierens, K., Burkhardt, U., and Smit, H.: A global climatology of upper-tropospheric ice supersaturation occurrence inferred from the Atmospheric Infrared Sounder calibrated by MOZAIC, Atmos. Chem. Phys., 12, 381–405, https://doi.org/10.5194/acp-12-381-2012, 2012.

Lee, D. S., Fahey, D. W., Skowron, A., Allen, M. R., Burkhardt, U., Chen, Q., Doherty, S. J., Freeman, S., Forster, P. M., Fuglestvedt, J., et al.: The contribution of global aviation to anthropogenic climate forcing for 2000 to 2018, Atmos. Environ., 244, 117 834, https://doi.org/10.1016/j.atmosenv.2020.117834, 2021.

Li, Y., Mahnke, C., Rohs, S., Bundke, U., Spelten, N., Dekoutsidis, G., Groß, S., Voigt, C., Schumann, U., Petzold, A., et al.: Upper-tropospheric slightly ice-subsaturated regions: frequency of occurrence and statistical evidence for the appearance of contrail cirrus, Atm. Chem. Phys., 23, 2251–2271, https://doi.org/10.5194/acp-23-2251-2023, 2023.

Liu, Y., Xu, T., and Liu, J.: Characteristics of the seasonal variation of the global tropopause revealed by COSMIC/GPS data, Advances in space research, 54, 2274–2285, https://doi.org/10.1016/j.asr.2014.08.020, 2014.

Lloyd, G., Gallagher, M., Choularton, T., Krämer, M., Andreas, P., and Baumgardner, D.: In situ measurements of cirrus clouds on a global scale, Atmosphere, 12, 41, https://doi.org/10.3390/atmos12010041, 2020.

Marenco, A., Thouret, V., Nédélec, P., Smit, H., Helten, M., Kley, D., Karcher, F., Simon, P., Law, K., Pyle, J., et al.: Measurement of ozone and water vapor by Airbus in-service aircraft: The MOZAIC airborne program, An overview, Journal of Geophysical Research: Atmospheres, 103, 25 631–25 642, https://doi.org/10.1029/98JD00977, 1998.

Meerkötter, R. and Vázquez-Navarro, M.: Earth's Radiation Budget: The Driver for Weather and Climate, in: Atmospheric Physics: Background–Methods–Trends, pp. 55–67, Springer, 2012.

Ng, K. S., Farooq, D., and Yang, A.: Global biorenewable development strategies for sustainable aviation fuel production, Renewable and Sustainable Energy Reviews, 150, 111 502, https://doi.org/10.1016/j.rser.2021.111502, 2021.

Ovarlez, J., Gayet, J.-F., Gierens, K., Ström, J., Ovarlez, H., Auriol, F., Busen, R., and Schumann, U.: Water vapour measurements inside cirrus clouds in Northern and Southern hemispheres during INCA, Geophys. Res. Lett., 29, 60–1, https://doi.org/10.1029/2001GL014440, 2002.

Peixoto, J. P. and Oort, A. H.: Physics of climate, 1992.

Petzold, A., Thouret, V., Gerbig, C., Zahn, A., Brenninkmeijer, C. A., Gallagher, M., Hermann, M., Pontaud, M., Ziereis, H., Boulanger, D., et al.: Global-scale atmosphere monitoring by in-service aircraft–current achievements and future prospects of the European Research Infrastructure IAGOS, Tellus B, 67, 28 452, https://doi.org/10.3402/tellusb.v67.28452,, 2015.

Petzold, A., Krämer, M., Neis, P., Rolf, C., Rohs, S., Berkes, F., Smit, H. G., Gallagher, M., Beswick, K., Lloyd, G., et al.: Upper tropospheric water vapour and its interaction with cirrus clouds as seen from IAGOS long-term routine in situ observations, Faraday Discussions, 200, 229–249, 2017.

Petzold, A., Neis, P., Rütimann, M., Rohs, S., Berkes, F., Smit, H. G., Krämer, M., Spelten, N., Spichtinger, P., Nédélec, P., et al.: Ice-supersaturated air masses in the northern mid-latitudes from regular in situ observations by passenger aircraft: Vertical distribution, seasonality and tropospheric fingerprint, Atmos. Chem. Phys., 20, 8157–8179, https://doi.org/10.5194/acp-20-8157-2020, 2020.

Ponater, M., Bickel, M., Bock, L., and Burkhardt, U.: Towards determining the contrail cirrus efficacy, Aerospace, 8, 42, https://doi.org/10.3390/aerospace8020042, 2021.

Rap, A., Forster, P., Jones, A., Boucher, O., Haywood, J., Bellouin, N., and De Leon, R.: Parameterization of contrails in the UK Met Office climate model, J. Geophys. Res., 115, https://doi.org/10.1029/2009JD012443, 2010.

Reutter, P., Neis, P., Rohs, S., and Sauvage, B.: Ice supersaturated regions: properties and validation of ERA-Interim reanalysis with IAGOS in situ water vapour measurements, Atmos. Chem. Phys., 20, 787–804, https://doi.org/10.5194/acp-20-787-2020, 2020.

Sahoo, S., Zhao, X., and Kyprianidis, K.: A review of concepts, benefits, and challenges for future electrical propulsion-based aircraft, Aerospace, 7, 44, https://doi.org/10.3390/aerospace7040044, 2020.

Schmidt, E.: Die entstehung von eisnebel aus den auspuffgasen von flugmotoren, Schriften der Deutschen Akademie der Luftfahrtforschung, Verlag R. Oldenbourg, München, Heft 44, 5, 1–15, 1941.

Schumann, U.: On conditions for contrail formation from aircraft exhausts, Meteorologische Zeitschrift, 5, 4–23, https://doi.org/10.1127/metz/5/1996/4, 1996.

Schumann, U.: A contrail cirrus prediction model, Geosci. Model Dev., 5, 543–580, https://doi.org/10.5194/gmd-5-543-2012, 2012.

Schumann, U., Bugliaro, L., Dörnbrack, A., Baumann, R., and Voigt, C.: Aviation contrail cirrus and radiative forcing over Europe during 6 months of COVID-19, J. Geophys. Res., 48, e2021GL092 771, https://doi.org/10.1029/2021GL092771, 2021.

Smit, H. G., Rohs, S., Neis, P., Boulanger, D., Krämer, M., Wahner, A., and Petzold, A.: Reanalysis of upper troposphere humidity data from the MOZAIC programme for the period 1994 to 2009, Atmos. Chem. Phys., 14, 13 241–13 255, https://doi.org/10.5194/acp-14-13241-2014, 2014.

Sourdeval, O., Gryspeerdt, E., Krämer, M., Goren, T., Delanoë, J., Afchine, A., Hemmer, F., and Quaas, J.: Ice crystal number concentration estimates from lidar–radar satellite remote sensing – Part 1: Method and evaluation, Atmos. Chem. Phys., 18, 14 327–14 350, https://doi.org/10.5194/acp-18-14327-2018, 2018.

Sperber, D. and Gierens, K.: Towards a more reliable forecast of ice supersaturation: concept of a one-moment ice-cloud scheme that avoids saturation adjustment, Atmos. Chem. Phys., 2023, 1–23, https://doi.org//10.5194/acp-23-15609-2023, 2023.

Spichtinger, P., Gierens, K., Leiterer, U., and Dier, H.: Ice supersaturation in the tropopause region over Lindenberg, Germany, Meteorologische Zeitschrift, 12, 143–156, https://doi.org/10.1256/qj.02.141, 2003a.

Spichtinger, P., Gierens, K., and Read, W.: The global distribution of ice-supersaturated regions as seen by the Microwave Limb Sounder, Q. J. R. Meteorol Soc, 129, 3391–3410, https://doi.org/10.1256/qj.02.141, 2003b.

Wolf, K., Bellouin, N., and Boucher, O.: Long-term upper-troposphere climatology of potential contrail occurrence over the Paris area derived from radiosonde observations, Atmos. Chem. Phys., 23, 287–309, https://doi.org/10.5194/acp-23-287-2023, 2023.